Geochimica et Cosmochimica Acta 385 (2024) 16–33

Contents lists available at ScienceDirect

Geochimica et Cosmochimica Acta

journal homepage: www.elsevier.com/locate/gca

Tracking subduction-related metasomatism of the subcontinental lithospheric mantle using Ca-, O-, and H-isotopes

S.E. Brooker [a,*], J.D. Barnes [a], J.C. Lassiter [a], A. Satkoski [a], D.G. Pearson [b]

[a] Department of Earth and Planetary Sciences, Jackson School of Geosciences, University of Texas at Austin, Austin, TX 78712, USA
[b] Department of Earth and Atmospheric Sciences, 1-26 Earth Sciences Building, University of Alberta, Edmonton, Alberta T6G 2E3, Canada

ARTICLE INFO

Associate Editor: Ralf Halama

Keywords:
Calcium isotopes
Oxygen and hydrogen isotopes
Mantle metasomatism
Recycled crustal signature
Peridotite xenoliths

ABSTRACT

Mantle xenoliths provide effective records of the metasomatic processes that affect continental lithosphere evolution, such as interaction with subducted components or modification via small-degree melts. Correlations between major/trace element geochemistry with stable and radiogenic isotope compositions can help constrain the source and timing of this metasomatism. We report new $\delta^{18}O$, $\delta^{44/40}Ca$, and δD values for twelve kimberlite-hosted mantle xenoliths from the Slave Craton (NWT, Canada), which show varying degrees of metasomatism. The $\delta^{18}O$ values of olivine ($\delta^{18}O_{ol} = +5.33 \pm 0.13‰$; 1σ; n = 12) overlap average mantle values. Clinopyroxene and garnet $\delta^{18}O$ values ($\delta^{18}O_{cpx} = +5.31 \pm 0.10‰$; $\delta^{18}O_{grt} = +5.37 \pm 0.23‰$; 1σ) extend below those reported in most mantle peridotites and are strongly correlated with clinopyroxene $\delta^{44/40}Ca$ (avg. = +1.00 ± 0.10‰; 1σ) and garnet $\delta^{44/40}Ca$ (avg. = +1.18 ± 0.19‰; 1σ) respectively, extending from typical mantle values to low $\delta^{18}O$ and high $\delta^{44/40}Ca$ values. In general, $\Delta^{18}O_{cpx\text{-}ol}$ and $\Delta^{18}O_{grt\text{-}ol}$ (ranging from −0.19‰ to +0.19‰ and from −0.56‰ to +0.35‰, respectively) are lower than expected equilibrium values at mantle temperatures. Strong negative correlations are found between $\delta^{18}O_{grt}$ and $\Delta^{18}O_{grt\text{-}ol}$ and garnet major and trace element composition (Na_2O, H_2O, La/Yb_N). Furthermore, phlogopite-bearing kelyphitic rims have δD values (avg. = −126 ± 13‰; 1σ) lower than typical mantle values. Whole rock Sm-Nd model ages and oxygen isotope diffusion modeling suggest that metasomatism occurred during the Mesozoic, shortly before kimberlite entrainment, consistent with indications from diamond-forming fluids from the Slave craton. The combined low $\delta^{18}O$, δD, and high $\delta^{44/40}Ca$ signature of the mantle peridotite xenoliths, along with the age constraints, suggest the metasomatic fluid/melt is sourced from a recycled oceanic crust component related to Mesozoic subduction in western North America.

1. Introduction

Mantle xenoliths are geochemical recorders of the mechanisms that form and modify the subcontinental lithospheric mantle (SCLM). We rely on xenoliths to understand the processes that affect the lithospheric mantle, such as decompression melting, subduction-related flux melting, metasomatism, and refertilization. These different processes distinctively alter the chemistry of mantle xenoliths before their eruption and allow for the identification of mantle processes that modified the SCLM.

Although elemental and radiogenic isotopes have been effective tracers of the impact of metasomatism on lithospheric materials (e.g., Menzies and Hawkesworth, 1987; Pearson and Wittig, 2014), they are limited in their ability to identify the source(s) of metasomatic fluids. Stable isotopes are a powerful tool for examining material fluxes between the Earth's surface and interior and thus provide a means of testing the sources of metasomatic fluids and whether recycled components are present in the SCLM. Stable isotope fractionation between mineral and melt phases at magmatic temperatures is small (e.g., <~0.5‰ for $\delta^{18}O$; Eiler, 2001; <~0.1‰ for $\delta^{44/40}Ca$; Zou et al., 2024), thereby providing little leverage for either partial melting or fractional crystallization to significantly affect isotope compositions. However, water–rock reactions at or near Earth's surface produce larger isotopic fractionations. Therefore, when surficial reservoirs (e.g., sediments, altered oceanic crust, serpentinites) are returned to the mantle via subduction, melts or fluids generated during the subduction process have the potential to interact with and change the isotopic composition of the overlying mantle wedge (e.g., Eiler, 2001; Sharp, 2017).

Although the mantle typically exhibits relative oxygen isotope

* Corresponding author.
E-mail addresses: sbrooker@utexas.edu (S.E. Brooker), jdbarnes@jsg.utexas.edu (J.D. Barnes), lassiter1@jsg.utexas.edu (J.C. Lassiter), satkoski@jsg.utexas.edu (A. Satkoski), gdpearson@ualberta.ca (D.G. Pearson).

https://doi.org/10.1016/j.gca.2024.09.036
Received 11 April 2024; Accepted 28 September 2024
Available online 3 October 2024

homogeneity, the range of $\delta^{18}O$ values in olivine from peridotite xenoliths (+4.7 to +8.0‰) and their standard deviation (±0.4‰) greatly exceed the method's analytical uncertainty (typically ≤ 0.1‰, 1σ) and the accepted value of mantle olivine (5.2 ± 0.1‰) as defined by Mattey et al. (1994). These subtle variations, detectable due to precise analytical methods, may reveal important underlying processes that have previously been overlooked. Surprisingly, only a few studies have paired mantle peridotite $\delta^{18}O$ values with trace element and radiogenic tracers to identify potential input of metasomatic fluids/melts related to subduction, but the studies that have done this have shown this approach to be highly effective (e.g., Hao et al., 2015; Marshall et al., 2017; Wang et al., 2018; Fitzpayne et al., 2019a). For example, Fitzpayne et al. (2019a) report negative correlations between $\delta^{18}O$ values and clinopyroxene (cpx) major and trace elements (Cr_2O_3, jadeite component, Mg#, La/Zr) in lherzolites from Bultfontein kimberlite (Kimberley, South Africa), which are interpreted to reflect mantle metasomatism from a melt containing a recycled ocean crust component. Moreover, oxygen isotope fractionation between coexisting mineral phases ($\Delta^{18}O_{x-y}$, where $\Delta^{18}O_{x-y} = \delta^{18}O_x - \delta^{18}O_y$) in over 50% of published data on mantle peridotites (i.e., Gregory and Taylor, 1986; Deines and Haggerty, 2000; Zhang et al., 2000; Orr and Luth, 2000; Perkins et al., 2006) are inconsistent with equilibrium fractionation suggested by theoretical calculations or experimental investigations (Chiba et al., 1989; Zheng, 1993; Rosenbaum et al., 1994). Several studies (e.g., Perkins et al., 2006) have attributed non-equilibrium $\Delta^{18}O_{px-ol}$ values measured in many xenolith suites to open-system metasomatic interaction with a low $\delta^{18}O$ fluid/melt that may preferentially affect the pyroxenes.

Non-traditional stable isotope systems, such as Ca, Mg, and Fe isotopes, have in recent years been increasingly applied to the study of mantle-derived xenoliths and igneous rocks (e.g., Wang et al., 2016; Liu et al., 2017; Chen et al., 2019; Soderman et al., 2021; Antonelli et al., 2023; Erikson et al., 2024), and can provide complementary constraints on the presence and nature of recycled components in the mantle to those offered by traditional radiogenic or oxygen isotope studies. In particular, several studies have suggested that mantle xenoliths with $\delta^{44/40}Ca$ values (+0.67 to +0.80‰) lower than fertile, unmetasomatized mantle ($\delta^{44/40}Ca = +0.94 \pm 0.1$‰; Chen et al., 2019) reflect mantle modification due to the subduction of carbonate sediments and altered oceanic crust (e.g., Liu et al., 2017), although several recent studies disagree with the carbonate subduction hypothesis (Antonelli et al., 2023; Zou et al., 2024, Eriksen et al., 2024). Despite the potential for

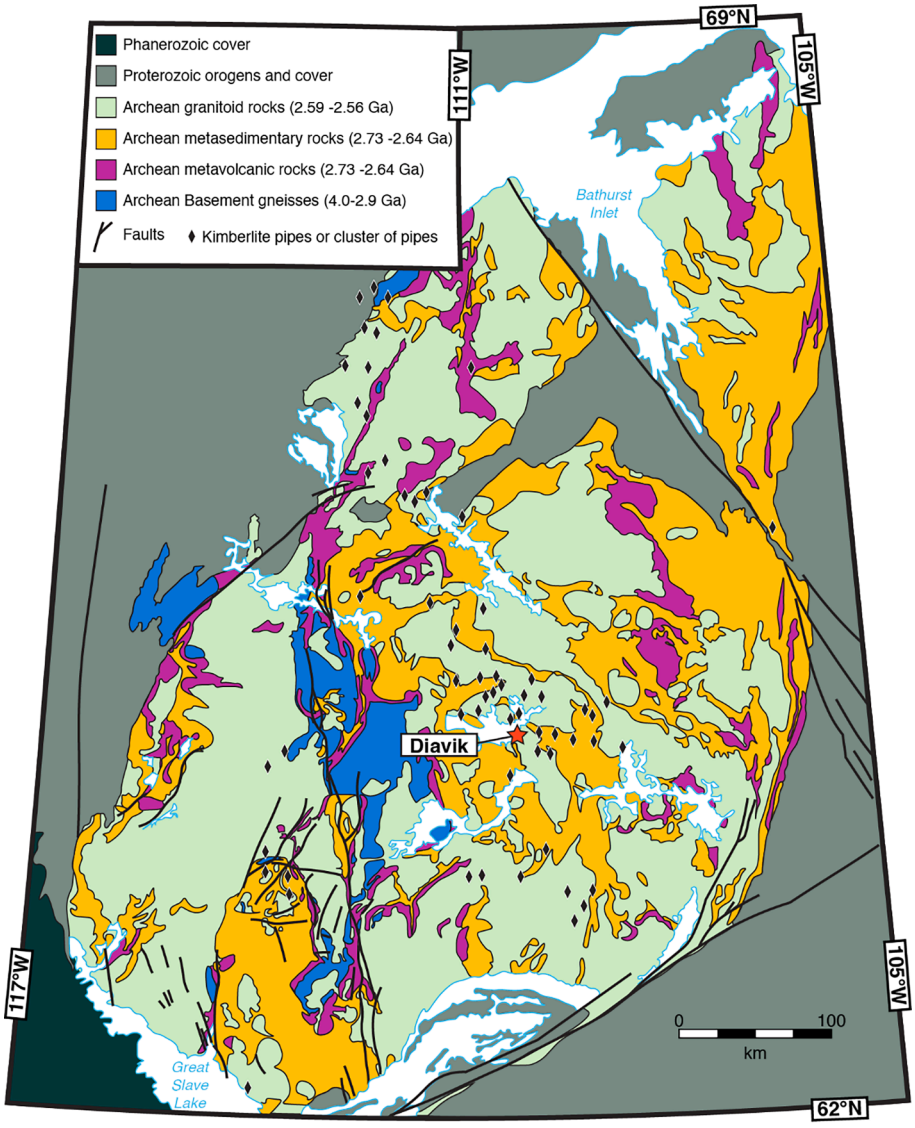

Fig. 1. Geologic map of the Slave craton showing the distribution of Mesoarchean basement, in blue. Adapted from Helmstaedt and Pehrsson (2012). The Diavik kimberlites from the Lac de Gras area are denoted with the red star.

stable isotopes to trace evidence of subduction into the mantle, no studies have examined O and Ca isotope covariations in the same mantle peridotite xenoliths. To our knowledge, only *one peridotite xenolith* has both published Ca and O isotope data, with the data published in separate studies ($\delta^{18}O = +5.3‰$; $\delta^{44/40}Ca = +0.99‰$; sample from Vitim, Siberia; Ionov et al., 1994; Kang et al., 2017).

Small isotopic variations reported in mantle peridotites may contain overlooked signals of subduction processes over geologic time. In this study, we pair stable isotope data with major and trace element geochemical data, combining $\delta^{18}O$, $\delta^{44/40}Ca$, and δD values with other geochemical tracers to evaluate the role subduction has played in modifying the elemental budgets of mantle xenoliths from the Archean Slave Craton located in the Northwest Territories, Canada. We seek to address the following questions: (1) Are there variations in the oxygen, hydrogen, and calcium isotope composition in mantle xenoliths from the Slave Craton? (2) If so, can variations and correlations between oxygen/hydrogen/calcium isotope ratios and other geochemical data, along with age constraints, be used to constrain the nature and source of the variability (i.e., sources from subducting sediments, subducting oceanic crust, or kimberlite melt)?

2. Geologic setting

The Slave craton, located in the Northwest Territories, Canada (Fig. 1) and exposed over 210,000 km^2, is a small Archean province within the larger North American craton (Isachsen and Bowring, 1994). Kimberlite emplacement spans a period of over 600 m.y. in at least five episodes of kimberlite magmatic activity from the late Proterozoic (616 Ma) to the Eocene (45 Ma) (Heaman et al., 2003; Kjarsgaard, 2007; Sarkar et al., 2015).

Recovery of mantle xenoliths from kimberlite drill cores provides direct samples of the Slave craton SCLM. Mineralogically, mantle xenoliths consists of forsterite olivine (ol), enstatite (opx), Cr-diopside (cpx), Ca-rich garnet (grt), chromite (chr), and kyanite (ky). Pearson et al. (1999) characterized several lithological groups from kimberlite pipes in the Lac de Gras area: lherzolites (ol + opx + cpx + grt ± chr), harzburgites (ol + opx + grt ± chr), dunites (ol ± grt ± chr), websterite (opx + cpx + grt ± chr), and eclogites (cpx + grt ± ky). Thermobarometry and mineral major and trace element compositions suggest a stratified SCLM with peridotites grouped into a low-temperature, shallow suite (<1000 °C, <145 km) and a high-temperature, deeper suite (1000–1400 °C, >145 km) (Griffin et al., 1999b, 1999a; Grütter et al., 1999; Pearson et al., 1999; Kopylova and Russell, 2000; Carbno and Canil, 2002; Kopylova and McCammon, 2003; Creighton et al., 2010; Aulbach et al., 2013). There is a pronounced contrast in chemical compositions between the shallow and deeper lithosphere. The shallow mantle shows greater chemical depletion (e.g., olivine Mg# ranges from 92 to 94) than the deeper layer (olivine Mg# ranges from 91 to 92).

About 30% of published Re-depletion ages of peridotite xenoliths from the Slave Craton range from 3.0 to 2.6 Ga, whereas the remaining have Re-depletion ages younger than 2.5 Ga, particularly in the North Slave Craton (Irvine, 2002; Liu et al., 2021). T_{RD} ages calculated from published peridotite Os data (Aulbach et al., 2004, 2009; Westerlund et al., 2006) from the central Slave region (Ekati and Diavik-born samples) have a peak age of around 2.75 Ga (n = 75). This age is interpreted to reflect when a large portion of the Slave SCLM formed and stabilized (Heaman and Pearson, 2010), and corresponds to when an active convergent margin coupled the western and eastern crustal domains at 2.6–2.7 Ga (i.e., Helmstaedt, 2009). Consistent with this, many studies have demonstrated that mantle eclogite and pyroxenite xenoliths from the shallow layer range from 1.8 to 2.7 Ga (i.e., Schmidberger et al., 2005, 2007; Aulbach et al., 2007; Smart et al., 2014, 2017). The shallower, spinel- and garnet-bearing peridotite layer (<145 km) generally yields older Archean-Proterozoic (between 3.0 Ga and 2.5 Ga) model ages (Irvine, 2002) than the deeper, younger Proterozoic (1.8 to 2.2 Ga) garnet-bearing peridotite layer (>145 km). This age stratification likely reflects either refertilization of the deeper mantle or an incremental downward growth of the SCLM (i.e., Griffin et al., 1999a).

The Slave SCLM shows extensive evidence for metasomatism and hydration (Araújo et al., 2009; Creighton et al., 2010; Aulbach et al., 2013; Kilgore et al., 2020). The shallow and deeper layers are thought to have had different metasomatizing agents due to differences in garnet trace element enrichments and depletions. Garnets from the shallow layer are enriched in LREE compared to MREE and HREE and have negative Sr, Zr, Hf, and Ti anomalies attributed to metasomatism by an oxidized carbonatite-like melt (Creighton et al., 2010; Aulbach et al., 2013). Shallow carbonatite metasomatism is identified by low Ti/Eu (<2500) and high Zr/Hf (>40) ratios in garnets (Shu and Brey, 2015). Aulbach et al. (2013) and Kilgore et al. (2020) suggest the deeper layers were metasomatized by evolving kimberlitic melts/fluids with lower LREE enrichment and Ti depletion and that this metasomatism also increased H concentrations in nominally anhydrous minerals.

2.1. Samples in this study

We analyzed twelve garnet-bearing mantle xenoliths (see Table S.1 for more details) from the Diavik A154N (samples with DDM prefix) and A154S (samples with MX prefix) kimberlite pipes located in the Lac de Gras area (Fig. 1). These xenoliths are predominantly composed of olivine, orthopyroxene, clinopyroxene, and garnet, with garnets exhibiting thick kelyphitic rims in most samples. These kimberlite pipes have an Rb-Sr age of 55.4 ± 0.4 Ma (Graham et al., 1999; Creaser et al., 2004). Based on calculated equilibration pressures and temperatures from the orthopyroxene-garnet barometer and the orthopyroxene-clinopyroxene thermometer of Brey and Köhler (1990), these xenoliths equilibrated in the deeper layer (from 181 to 214 km) at pressures ranging from 5.3 GPa to 6.8 GPa and temperatures ranging from 1200 °C to 1332 °C (Creighton et al., 2010; Kilgore et al., 2020; Table S.1). Previous work on these samples by Creighton et al. (2010), Mather (2012), and Kilgore et al. (2020) report olivine and orthopyroxene Mg numbers (100× [Mg/(Mg + Fe)]) ranging from 90.1 to 91.6 and 91.3 to 92.9, respectively.

Nominally anhydrous minerals present in these xenoliths (olivine, clinopyroxene, and garnet) contain 31–74, 104–284, and 1–54 μg/g H_2O, respectively (Kilgore et al., 2020). Kilgore et al. (2020) identified correlations between mineral hydrogen contents and tracers of metasomatism (i.e., garnet LREE/HREE ratios). They attributed these correlations to the effects of percolation of kimberlite-like melts through garnet peridotite. However, the timing and source of this metasomatism is unconstrained.

Previous studies noted the absence of hydrous minerals such as phlogopite or amphibole in these samples (Creighton et al., 2010). However, we document the presence of garnets with thick kelyphitic rims (0.1 mm to 0.5 mm), opaque in thin section (Fig. S.1), bearing abundant phlogopite in all samples. Samples DDM_149 and DDM_327 have thinner rims (<0.1 mm; Fig. S.2). Kelyphites are fine-grained rims of a mixture of spinel, olivine, and pyroxene and can contain hydrous mineral phases such as amphiboles and phlogopite if sufficient water is present (Obata, 1994; Godard and Martin, 2000; Pokhilenko, 2021). The kelyphitic rims in samples from this study consist of fine-grained opaque minerals with large grains of phlogopite (Figs. S.1 and S.2). Kelyphitic rims surrounding garnets are thought to form either (1) as a result of a reaction between garnet and adjacent minerals (olivine, pyroxene) or (2) as a result of garnet decompression (Obata, 1994; Godard and Martin, 2000; Dégi et al., 2010).

3. Methods

The garnet peridotite samples were prepared for mineral separation by cleaning the samples manually and removing any significant vein material by sawing. For mineralogy, geochemical, and isotopic analysis, minerals were separated as follows. Bulk xenoliths were gently

disaggregated using a rock hammer. Mineral separates (olivine, clinopyroxene, and garnet) were hand-picked under a binocular microscope. Only the cleanest, "gem"-like, alteration- and inclusion-free grains were selected. Mineral separates were cleaned for several hours in 2 N HCl, ultrasonicated, and rinsed in de-ionized water. Hydrous, multi-mineral kelyphitic rims were hand-picked under a binocular microscope and not treated with HCl or water. Samples DDM_359 and DDM_384 did not have previously published mineral major element data. Therefore, mineral separates were picked and mounted in epoxy for electron microprobe analysis. Electron microprobe methods and data are in the Supplemental Information and Tables S2 and S3. Phlogopite was identified as one of the mineral phases present in the kelyphitic rim matrix during electron microprobe work (Supplemental Information Section S.2).

3.1. Oxygen Isotope Analysis

Oxygen isotope ratios were measured in the stable isotope laboratory at the Jackson School of Geoscience, University of Texas at Austin, using a ThermoElectron MAT 253 mass spectrometer. $\delta^{18}O$ values of silicate minerals were measured using the laser fluorination method outlined in Sharp (1990). Laser fluorination requires small amounts of pure silicate mineral separates (~2 mg). All $\delta^{18}O$ values are reported relative to standard mean ocean water (SMOW; $\delta^{18}O_{SMOW} \equiv 0‰$). To check for precision and accuracy, garnet UWG-2 ($\delta^{18}O = +5.8‰$; Valley et al., 1995), in-house olivine San Carlos ($\delta^{18}O = +5.3‰$), and quartz Lausanne-1 ($\delta^{18}O = +18.1‰$) standards were run with each batch of sample analyses. Mineral separates were analyzed one to five times; most were analyzed more than once. The data presented here is the mean value of multiple analyses, and the uncertainty is reported as one standard deviation of the multiple analyses. Garnet standard UWG-2 had an average precision throughout the analytical runs of ±0.07‰ (1σ). Precision for olivine and garnet analyses of xenolith samples is ±0.06‰ based on the reproducibility of replicated samples. Precision for clinopyroxene minerals is lower, averaging ±0.31‰, likely due to the inability to pick inclusion-free grains. Clinopyroxene separates are very dark, making it challenging to detect minor spinel inclusions.

The presence of Cr_2O_3 in minerals can hinder the total fluorination of samples, particularly in garnet (Cr_2O_3 ranges from 2 to 10 wt%). The $\delta^{18}O_{grt}$ value was corrected by increasing the overall measured value by 0.064‰ per weight percentage of Cr_2O_3, following Wang et al. (2011). The correction for each analysis is shown in Table S.4 and the standard deviation of all garnet analyses decreases from 0.35‰ in uncorrected values to 0.22‰ in corrected values. All of the $\delta^{18}O_{grt}$ data presented in the results and the discussion are the corrected $\delta^{18}O_{grt}$ values.

3.2. Calcium isotope analysis

Minerals with significant concentrations of Ca (i.e., clinopyroxene and garnet) were analyzed for their Ca isotope composition. Individual mineral separates were powdered and dissolved in a 3:1 HF-HNO3 acid mixture in Teflon beakers for ~5 days. Samples were then taken to dryness. Once dry, 6 M HCl was added, and samples were heated until the sample was fully dissolved. Samples were taken to dryness and then dissolved in 2.5 M HCl to make a ~200 ppm Ca solution. From this ~200 ppm Ca solution, 10 µg of Ca was aliquoted and mixed with a ^{42}Ca-^{48}Ca double spike. The sample/spike mixture was taken to dryness, then dissolved in 100 µl of 2.5 M HCl to prepare them for ion-exchange chemistry. The ion exchange chemistry is modified from Huang et al. (2011) and briefly described here. Calcium was separated from the matrix using 250 µl of BioRad AG50W-X12 (200–400 mesh) cation exchange resin loaded into a custom-made Teflon column. Calcium was eluted using 1.1 ml of 2.5 M HCl. The full ion exchange separation was performed twice. Ca yields are estimated to be greater than 94%. Procedural blanks are insignificant for the amount of Ca processed for each sample (10 µg), based on analyses of similar quantities of Ca from known rock standards that were processed with each column batch of unknowns.

Samples were then loaded onto outgassed Re filaments using 2.5 M HCL and 1 M H_3PO_4 before being put into a Thermo Scientific Triton TIMS (thermal ionization mass spectrometer) and analyzed at the University of Texas-Austin. The TIMS lab utilizes a double-filament geometry for the analysis of Ca isotopes. The samples were analyzed in 5 blocks of 20 cycles with signal intensity of $\sim 1 \times 10^{-10}$ amps of ^{40}Ca. All peaks were measured on Faraday cups using 10^{11} ohm resistors. The data collection was done with a peak hopping routine where ^{40}Ca, ^{42}Ca, ^{43}Ca, ^{44}Ca were measured in the first sequence and ^{44}Ca and ^{48}Ca in the second sequence. The double spike inversion follows that outlined by Rudge et al. (2009). The $\delta^{44/40}Ca$ was calculated and normalized using our long-term (~2 year) spiked and unspiked NIST SRM 915a measurements. Samples that were analyzed once are assigned an uncertainty of ±0.1‰ (2SD) based on the reproducibility of spiked NIST SRM 915a measurements over a range of spike/sample ratios. Samples analyzed more than once (repeated measures of a sample loaded onto a single filament) were assigned a 2SE based on the repeated measurements. International peridotite rock standard JP-1 was analyzed and produced a $\delta^{44/40}Ca = 1.09 \pm 0.1‰$ (2SD), consistent with published values (e.g., Magna et al., 2015; He et al., 2017).

3.3. Hydrogen isotope analysis

The hydrogen isotope ratios of hydrous, multi-mineral kelyphitic rims around garnets were determined using the methods of Sharp et al. (2001). Because of their fine-grained nature, we measured the kelyphitic rims as a whole, rather than individual phlogopite grains. Approximately 6 mg of kelyphitic rims were crushed and loaded in silver foil capsules. All samples were dried overnight at 100 °C in a vacuum furnace to remove surface water before pyrolysis in a ThermoElectron MAT TC-EA, coupled to a ThermoElectron MAT 253 mass spectrometer located in the stable isotope laboratory at the Jackson School of Geosciences, University of Texas at Austin. All δD values are reported relative to SMOW (0‰). Analyses of standards NBS-22, CH7, USGS 57, and USGS 58 were used to construct a δD calibration curve. Error on each δD analysis is ±2‰ (1σ). Duplicate sample measurements are reported in Table S.7.

3.4. Samarium-neodymium analysis

Sm-Nd isotopes were measured on ~10 to ~50 mg of hand-picked cpx and garnet separates from 5 xenoliths. Samples were spiked with an enriched ^{149}Sm-^{150}Nd mixed spike and dissolved using 29 M HF and 15 M HNO3. The bulk REEs were extracted via ion exchange chemistry using AG50W-X8 and 6 M HCl. Neodymium was separated from Sm using LN-Spec resin and 0.6 M and 0.3 M HCl. Nd fractions were loaded onto an outgassed Re filament and analyzed using a double filament geometry on a Thermo Fisher Triton TIMS at the University of Texas-Austin. Samarium measurements were made on a Nu Plasma 3D MC-ICPMS at the University of Texas at Austin. Correction for mass bias was done by the sample-standard bracketing technique using a purified Sm standard. The long-term value and precision for isotope standard JNdi-1 measured by the laboratory produces a $^{143}Nd/^{144}Nd$ ratio of 0.512113 ± 0.000013 (2SD; n = 42), consistent with published values for this standard (e.g., Tanaka et al., 2000). Rock standard BHVO-2 analyzed during this study produced a $^{143}Nd/^{144}Nd$ ratio of 0.513002 and a $^{147}Sm/^{144}Nd$ ratio of 0.1495, consistent within the uncertainty of published values.

4. Results

4.1. $\delta^{18}O$ values of olivine, clinopyroxene, and garnet

Peridotites from the lower Slave lithospheric mantle have an average

$\delta^{18}O_{ol}$ value of +5.33 ± 0.13‰ (1σ; n = 12), with a range of +5.02 to +5.51‰ (Fig. 2a, Tables 1 and S.8). This range is within the error of the previously reported average mantle olivine (+5.2 ± 0.3‰ 1σ; Mattey et al., 1994). Our newly acquired data agree with existing SIMS data from Regier et al. (2018) on Archean cratonic peridotite xenoliths and span a similar range of $\delta^{18}O_{ol}$ values (+5.01 to +5.53‰; n = 22). We reanalyzed six samples from Regier et al. (2018) and reproduced their published values within error, except for sample DDM_327 (Fig. S.3), where Regier et al. (2018) report a $\delta^{18}O_{ol}$ = +5.15‰, and we measured $\delta^{18}O_{ol}$ = +5.48‰). Bulk analyses of DDM_327 olivine of three separate measurements yielded an error of ±0.03‰ (1σ) (Table S.8).

In contrast, clinopyroxene and garnet have oxygen isotope compositions that extend to values lower than typical for mantle peridotites. $\delta^{18}O_{cpx}$ values range from +5.10‰ to +5.43‰, with an average of +5.31 ± 0.10‰ (1σ; Fig. 2a; Tables 1 and S.9). Clinopyroxenes from samples MX158, DDM_335, DDM_360, and DDM_384 have $\delta^{18}O_{cpx}$ values lower than the reported average mantle clinopyroxene values (+5.57 ± 0.16‰; 1σ; Mattey et al., 1994). $\delta^{18}O_{grt}$ values have an average of +5.37 ± 0.23‰ (1σ) and range from +4.95‰ to +5.65‰ (Fig. 2a; Tables 1 and S.4). Garnets from samples MX158, MX5001, MX5020, DDM_361, DDM_367, and DDM_368 have $\delta^{18}O_{grt}$ values lower on average than reported mantle garnet values (+5.5 to +6.0‰; Ionov et al., 1994).

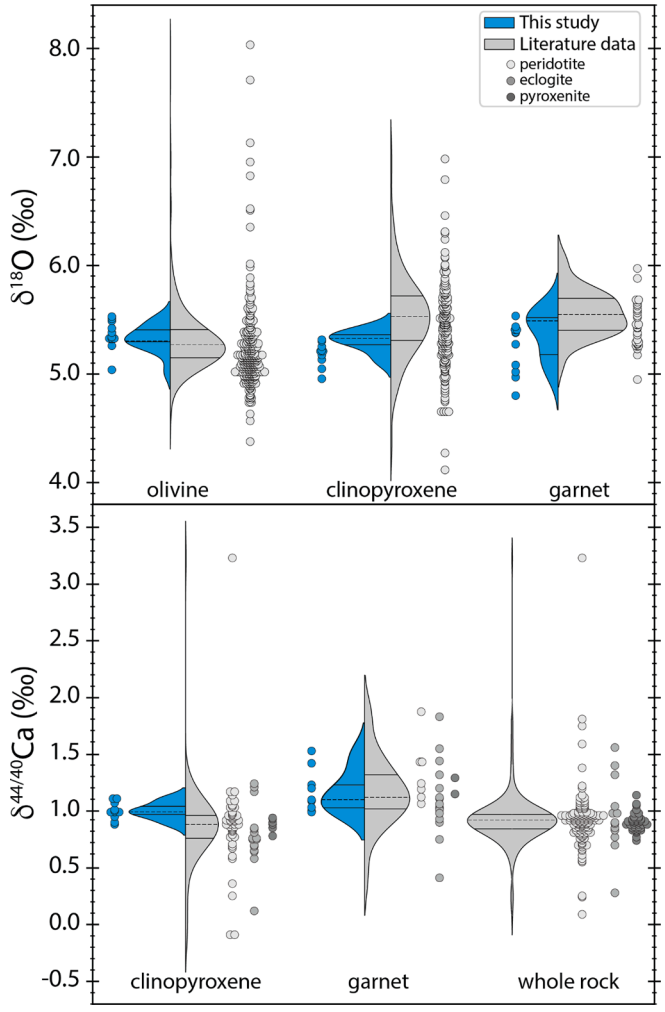

Fig. 2. (a) Violin plot of mineral $\delta^{18}O$ values (‰) from this study (in blue) compared to published literature peridotite mineral $\delta^{18}O$ values (‰; light gray; Mattey et al., 1994; Ionov et al., 1994; Chazot et al., 1997; Lowry et al., 1999; Deines & Haggerty, 2000; Zhang et al., 2000; Perkins et al., 2006; Rehfeldt et al., 2008; Wang et al., 2011; Liu et al., 2014; Hao et al., 2015; Marshall et al., 2017; Polat et al., 2018; Reiger et al., 2018; Wang et al., 2018; Dallai et al., 2019; Fitzpayne et al., 2019; Lebedeva et al., 2020) and (b) violin plot of $\delta^{44/40}Ca$ values (‰) from this study (in blue) compared to published literature peridotite, eclogite, and pyroxenite mineral and whole rock $\delta^{44/40}Ca$ (‰; Huang et al., 2010; Kang et al., 2016, 2017; Zhao et al., 2017; Chen et al., 2018; Amsellem et al., 2019; Antonelli et al., 2019; Chen et al., 2019; Ionov et al., 2019; Kang et al., 2019; Wang et al., 2019; Dai et al., 2020; Kang et al., 2020; Smart et al., 2021; Tappe et al., 2021). Dashed line represents the median and solid lines represent the upper and lower quartiles.

For the Slave peridotites, the measured fractionation between clinopyroxene and olivine ($\Delta^{18}O_{cpx\text{-}ol}$) ranges from −0.18‰ to +0.19‰ (Table 1), with all $\Delta^{18}O_{cpx\text{-}ol}$ values lower than expected equilibrium fractionation at mantle temperature ranges from this study (Fig. 3a; 1200–1400 °C; $\Delta^{18}O_{cpx\text{-}ol}$ = +0.30 to +0.40‰; Chiba et al., 1989; Rosenbaum et al., 1994; Valley, 2003). The measured fractionation between garnet and olivine minerals ($\Delta^{18}O_{grt\text{-}ol}$) ranges from −0.56‰ to +0.35‰ (Table 1), which is also lower than predicted equilibrium fractionation at mantle temperatures from this study (Fig. 3b; 1200–1400 °C; $\Delta^{18}O_{grt\text{-}ol}$ = +0.40 to +0.60‰; Zheng, 1993). The fractionation between garnet and clinopyroxene minerals ($\Delta^{18}O_{grt\text{-}cpx}$) ranges from −0.38‰ to +0.47‰ (Table 1). Most samples fall within the predicted equilibrium fractionation range at mantle temperatures from this study (Fig. 3c; 1200–1400 °C; $\Delta^{18}O_{grt\text{-}cpx}$ = 0.00 to +0.20‰; Zheng, 1993), except for three samples, DDM_149, DDM_361, and DDM_367 (Table 1). The observed oxygen isotope equilibrium between garnet and clinopyroxene is supported by the calculated trace element distribution coefficients, which are consistent with equilibrium values (Fig. S.4).

4.2. $\delta^{44/40}Ca$ values of clinopyroxene and garnet

The average clinopyroxene $\delta^{44/40}Ca_{cpx}$ value is +1.00 ± 0.07‰ (1σ), ranging from +0.88‰ to +1.11‰ (Table 2; Fig. 2b), with all individual samples within uncertainty of the average MORB-source mantle, $\delta^{44/40}Ca$ = +0.94 ± 0.10‰ (Chen et al., 2019). $\delta^{44/40}Ca_{grt}$ values record a wider range (+0.99‰ to +1.53‰) than clinopyroxene, with an average of +1.18 ± 0.19‰ (1σ; Table 2; Fig. 2b). Most garnets in this study have higher $\delta^{44/40}Ca$ values than bulk peridotite values ($\delta^{44/40}Ca$ = +0.94 ± 0.10‰; Chen et al., 2019). However, samples have similar $\delta^{44/40}Ca_{grt}$ values compared to garnets in mantle peridotites (Fig. 2b; $\delta^{44/40}Ca_{grt}$ = +1.33 ± 0.28‰; 1σ; n = 7; Wang et al., 2019; Tappe et al., 2021), garnets in mantle pyroxenites (Fig. 2b; $\delta^{44/40}Ca_{grt}$ = +1.22 ± 0.09‰; 1σ; n = 2; Dai et al., 2020) and garnets in mantle eclogites (Fig. 2b; $\delta^{44/40}Ca_{grt}$ = +1.10 ± 0.33‰; 1σ; n = 16; Antonelli et al., 2019; Kang et al., 2019; Smart et al., 2021).

The fractionation between garnet and clinopyroxene ($\Delta^{44/40}Ca_{grt\text{-}cpx}$) in peridotites is not well constrained. Measured fractionations in this study ($\Delta^{44/40}Ca_{grt\text{-}cpx}$ values = 0.00‰ to +0.52‰; average = +0.18 ± 0.17‰; 1σ; Table 2, Fig. 4) are lower than the average measured fractionations for peridotites, but are within 1 standard deviation ($\Delta^{44/40}Ca_{grt\text{-}cpx}$ = +0.48 ± 0.28‰; 1σ; n = 7; Wang et al., 2019; Tappe et al., 2021). For context, in mantle pyroxenites, average $\Delta^{44/40}Ca_{grt\text{-}cpx}$ values equal +0.33 ± 0.16‰ (1σ; n = 2; Dai et al., 2020). Eclogites have an average $\Delta^{44/40}Ca_{grt\text{-}cpx}$ values equal to +0.30 ± 0.11‰ (1σ; n = 15; Kang et al., 2019; Smart et al., 2021). Theoretical calculations predict $\Delta^{44/40}Ca_{grt\text{-}cpx}$ values to range from +0.20 to +0.35‰ at mantle temperatures, 1000–1400 °C (Huang et al., 2019; Antonelli et al., 2019).

There are negative correlations (r^2 = 0.35 and 0.69 and p = 0.123 and 0.006, respectively) between the $\delta^{44/40}Ca_{cpx}$ and $\delta^{18}O_{cpx}$ values and between $\delta^{44/40}Ca_{grt}$ and $\delta^{18}O_{grt}$ values (Fig. 5).

4.3. δD values of kelyphitic rims

The kelyphitic rims have an average δD value of −126 ± 13‰ (1σ), ranging between −145‰ and −106‰ (Table 3; Fig. 6). These values are more negative than the average MORB sourced-mantle values (−80 ± 5‰; Fig. 6; Kyser and O'Neil, 1984). The kelyphite values are also lower than those measured in phlogopites from mantle xenoliths from

Table 1
$\delta^{18}O$ values for mineral separates.

Sample	Average $\delta^{18}O_{ol}$ (‰)	1 s.d. (‰)	Average $\delta^{18}O_{cpx}$ (‰)	1 s.d. (‰)	Corrected $\delta^{18}O_{grt}$ (‰)	1 s.d. (‰)	$\Delta^{18}O_{cpx\text{-}ol}$ (‰)	1 s.d. (‰)	$\Delta^{18}O_{grt\text{-}ol}$ (‰)	1 s.d. (‰)	$\Delta^{18}O_{grt\text{-}cpx}$ (‰)	1 s.d. (‰)
MX158	5.02	0.15	5.10	0.10	5.15	0.13	0.08	0.18	0.13	0.20	0.05	0.16
MX5001	5.23	0.11	5.42	0.05^	5.49	0.01	0.19	0.12	0.26	0.11	0.07	0.05
MX5020*	5.29	0.06			5.10	0.04			−0.19	0.07		
DDM_149	5.30	0.03	5.18	0.04^	5.65	0.02	−0.12	0.05	0.35	0.04	0.47	0.04
DDM_327	5.48	0.03	5.33	0.18	5.52	0.08	−0.15	0.18	0.04	0.09	0.19	0.20
DDM_335	5.30	0.07	5.34	0.04^	5.52	0.08	0.04	0.08	0.22	0.11	0.18	0.09
DDM_359*	5.39	0.12			5.50	0.06			0.11	0.13		
DDM_360	5.35	0.01	5.37	0.04^	5.55	0.01	0.02	0.04	0.20	0.01	0.18	0.04
DDM_361	5.51	0.04	5.33	0.04	4.95	0.11	−0.18	0.06	−0.56	0.12	−0.38	0.12
DDM_367	5.30	0.04	5.43	0.28	5.21	0.18	0.13	0.28	−0.09	0.18	−0.22	0.33
DDM_368	5.31	0.04	5.26	0.30	5.39	0.08	−0.05	0.30	0.08	0.09	0.13	0.31
DDM_384**	5.46	0.08	5.30	0.10^			−0.16	0.13				
Average	5.33		5.31		5.37		−0.02		0.05		0.07	
1 s.d.	0.13		0.10		0.23		0.13		0.25		0.25	

* Insufficient cpx for oxygen isotope analysis.
** Insufficient garnet for oxygen isotope analysis.
^ Uncertainty is 1 s.d. of the UWG standard from that analytical session

kimberlites globally (avg. = −65 ± 12‰; Fig. 6; Sheppard and Epstein, 1970; Sheppard and Dawson, 1975; Kuroda et al., 1975, 1977; Boettcher and O'Neil, 1980; Banerjee et al., 2018). Phlogopitic rims from this study are more similar to δD values of K-richterite amphiboles in peridotites and MARID xenoliths from South Africa (avg. = −100 ± 24‰; Fig. 6; Kuroda et al., 1975; Banerjee et al., 2018).

4.4. Sm-Nd isotopes in clinopyroxene and garnet

Sm-Nd isotopic data were obtained for mineral separates of five samples (of which only garnet could be separated from DDM_327 and clinopyroxene from DDM_361; Table 4). Clinopyroxene has $^{147}Sm/^{144}Nd$ from 0.0680 to 0.1024 and yielded measured $^{143}Nd/^{144}Nd$ from 0.512170 to 0.512587. This corresponds to an ε_{Nd} (per 10,000 deviation from $^{143}Nd/^{144}Nd$ in a model chondritic source) from −9.2 to −1.0. In garnet mineral separates, $^{147}Sm/^{144}Nd$ is higher than clinopyroxene, ranging from 0.2721 to 0.3924. Garnet $^{143}Nd/^{144}Nd$ span a wider range than in clinopyroxene, ranging from 0.511793 to 0.512687, corresponding to ε_{Nd} from −16.5 to 0.9. Whole rock $^{147}Sm/^{144}Nd$ and $^{143}Nd/^{144}Nd$ were calculated from mineral Sm-Nd data (Table 4) and modal mineral compositions of peridotites (Table S.10) and are given in Table 5 for samples MX158 and DDM_367. The determination of mineral modal abundance is explained in Supplemental Information Section S.4.

5. Discussion

5.1. Evidence for subduction-related metasomatism

5.1.1. Calcium and oxygen isotope evidence for recycled crustal component

Metasomatism by a recycled crustal component is a reasonable explanation for non-mantle-like variations in the $\delta^{18}O$ and $\delta^{4/40}Ca$ values of some xenoliths. In Fig. 5, there are negative correlations between $\delta^{18}O_{cpx}$ and $\delta^{44/40}Ca_{cpx}$ values (with outlier clinopyroxene sample MX158 excluded, p-value = 0.123) and between $\delta^{18}O_{grt}$ and $\delta^{44/40}Ca_{grt}$ values (p-value = 0.0056) that trend from average mantle values ($\delta^{18}O_{cpx}$ = +5.42‰, $\delta^{18}O_{grt}$ = +5.49‰, $\delta^{44/40}Ca_{grt}$ = +1.00‰) to a reservoir with lower $\delta^{18}O$ values and higher $\delta^{44/40}Ca$ values ($\delta^{18}O_{cpx}$ = +5.10‰, $\delta^{18}O_{grt}$ = +4.95‰, $\delta^{44/40}Ca_{grt}$ = +1.53‰) which are end member values from this study. Smart et al. (2021) identified a similar negative correlation between $\delta^{18}O_{grt}$ and $\delta^{44/40}Ca_{grt}$ values in kimberlite-hosted eclogite xenoliths from the Kaapvaal Craton (Fig. 5; gray stars) and attributed this to either seawater alteration of oceanic crust protoliths or mixing between fresh and altered oceanic crustal protoliths. The higher $\delta^{44/40}Ca_{grt}$ values (>+1.3‰) were attributed to partial melting of eclogites (Smart et al., 2021), even though these samples have low $\delta^{18}O_{grt}$ values.

Partial melting results in minor stable O and Ca isotope fractionation in melt residues to lower $\delta^{18}O$ and higher $\delta^{44/40}Ca$ values. Hence, melting followed by melt extraction could produce the observed Ca-O isotope trends in Fig. 5. However, several lines of evidence suggest this is not the case for our study. Models of batch, fractional, and flux melting of lherzolitic peridotite indicate minimal oxygen isotopic fractionation in coexisting minerals, melt, and the residual bulk solid at temperatures greater than 1100 °C (approximately $\Delta^{18}O_{bulk\ original\text{-}residue}$ = +0.20‰ at 45% melt depletion and extraction; Bindeman et al., 2022). However, the degree of melt depletion observed in xenoliths from this study is significantly less than the 45% required to shift $\delta^{18}O$ by 0.20‰, and garnet minerals on average have $\delta^{18}O$ values 0.54‰ lower than what they would be if they were in equilibrium with their coexisting olivine. So even though $\delta^{18}O_{grt}$ values cover a narrow range, they still cannot be explained fully by partial melting. Additionally, partial melting of lherzolitic peridotites is expected to produce only small Ca isotope fractionations (~0.1‰; Zou et al., 2024) that do not fully explain the 0.54‰ variation in $\delta^{44/40}Ca_{grt}$ values in this study. If melting were the primary factor, we would expect to see a correlation between Ca and O isotopes and indices of melt extraction (i.e., Mg# in olivine and bulk Al_2O_3 concentrations), which is not observed in our data (Fig. S5). Instead, the correlations we observe between $\delta^{18}O_{grt}$, $\delta^{44/40}Ca_{grt}$, and elements like La/Yb, Na_2O, and H_2O indicate that metasomatism, rather than partial melting, is responsible for the isotopic variations in our study (Fig. 7).

Instead, several lines of evidence suggest that the correlated variations in Ca and O isotopes are most likely explained by metasomatism by an isotopically distinct melt or fluid that has incorporated recycled crustal components. Possible metasomatic sources include (1) subducted marine carbonates, (2) carbonatite magmatism, (3) subducted altered oceanic crust, and (4) subducted serpentinites. This fluid must travel through the mantle without having its O and Ca isotope composition significantly buffered by the ambient mantle it passes through.

Subducted carbonate appears unlikely to account for the observed trends because although marine carbonates span a wide range of $\delta^{44/40}Ca$ values (from −1.09‰ to +2.51‰; Fantle and Tipper, 2014), they typically have high $\delta^{18}O$ values, ranging from +20‰ to +40‰ (e.g., Mozley and Burns, 1993). Therefore, incorporating carbonate sediments into the mantle via subduction could raise or lower the $\delta^{44/40}Ca$ value of the mantle, but is expected to increase the $\delta^{18}O$ value of the mantle. Because high $\delta^{18}O$ values are not observed in our samples, they likely were not metasomatized by a fluid/melt derived from a subducted component dominated by marine carbonates.

Carbonatites are igneous rocks with more than 50% carbonate-

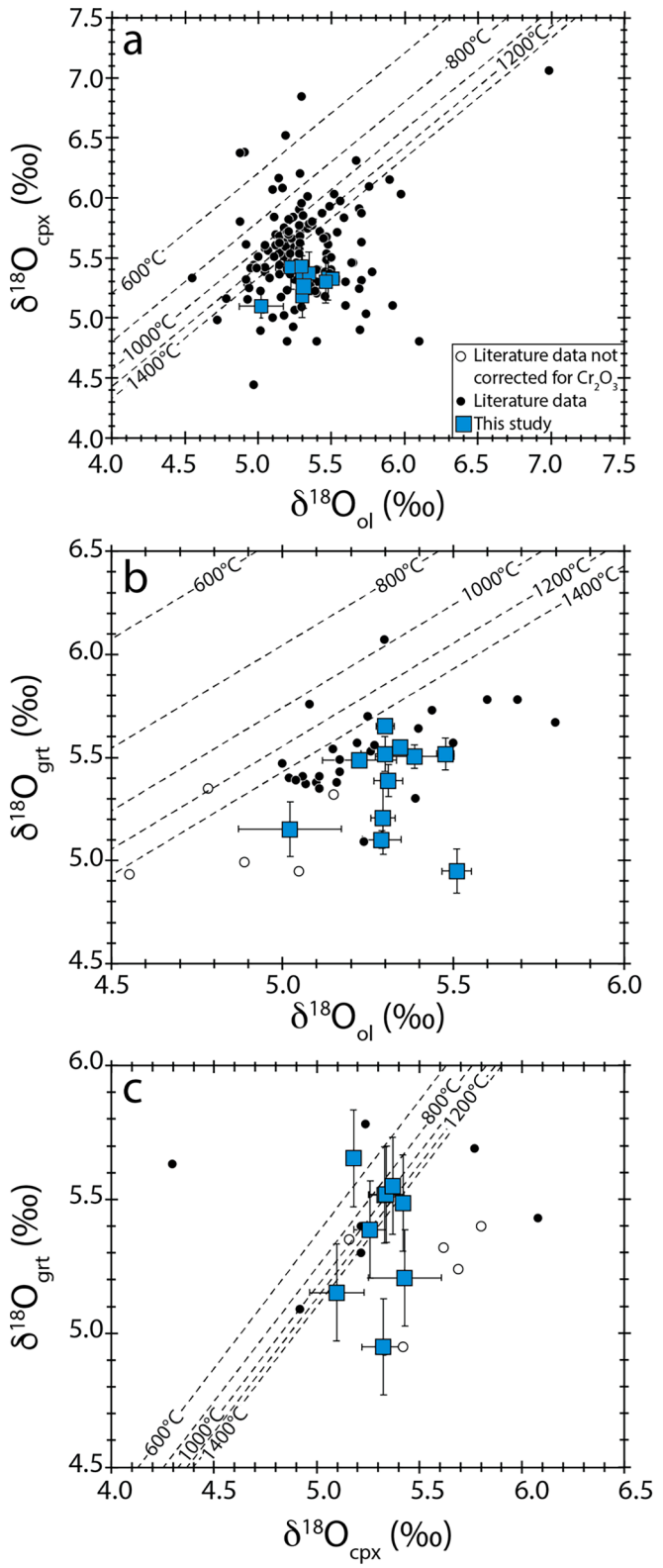

Fig. 3. (a) $\delta^{18}O_{cpx}$ (‰) vs. $\delta^{18}O_{ol}$ values (‰), (b) $\delta^{18}O_{grt}$ (‰)vs. $\delta^{18}O_{ol}$ (‰) and (c) $\delta^{18}O_{grt}$ (‰) vs. $\delta^{18}O_{cpx}$ (‰) values from this study compared to mineral $\delta^{18}O$ values of previously published peridotites (Mattey et al., 1994; Ionov et al., 1994; Chazot et al., 1997; Lowry et al., 1999; Deines & Haggerty, 2000; Zhang et al., 2000; Perkins et al., 2006; Rehfeldt et al., 2008; Wang et al., 2011; Hao et al., 2015; Polat et al., 2018; Dallai et al., 2019; Fitzpayne et al., 2019; Lebedeva et al., 2020) and equilibrium isotope fractionation for temperatures ranging from 600 °C to 1400 °C (Chiba et al., 1989; Zheng, 1993; Valley, 2003).

bearing minerals, and whether they originate from a primary mantle source or recycling of surface materials is still debated. Regardless, carbonatite magma can modify the surrounding mantle during ascent with a distinctive low $\delta^{44/40}$Ca value of +0.26 ± 0.25‰ (2σ; n = 50; Amsellem et al., 2020) and higher $\delta^{18}O$ value ranging from +6 to +10‰ (Horstmann and Verwoerd, 1997; Fig. 5). While the average carbonatite $\delta^{18}O$ value is higher than typical mantle values, equilibrium isotope fractionation between forsterite and calcite is ~−2‰ at mantle temperatures (Chiba et al., 1989) supports their derivation from a mantle source. Metasomatism by carbonatite magmas would lower the $\delta^{44/40}$Ca value and raise or not change the $\delta^{18}O$ value of the mantle. Since this is not observed in our samples, they likely were not metasomatized by a fluid/melt derived from a carbonatite magma.

Altered oceanic crust is also a possible source of non-mantle like $\delta^{18}O$ and $\delta^{44/40}$Ca values. On average, altered oceanic crust has a slightly higher Ca isotope composition than the average mantle, $\delta^{44/40}Ca = +1.03 \pm 0.19$‰, and spans a wider range than the average mantle value, from +0.54‰ to +1.23‰ (John et al., 2012; Blättler and Higgins, 2017). The bulk oxygen isotope composition of altered oceanic crust overlaps with average mantle values ($\delta^{18}O_{mantle} = +5.2 \pm 0.3$‰; Mattey et al., 1994) and ranges from ~0 to +5.5‰ in altered sheeted dike complexes, ~+2 to +5.5‰ in hydrothermally altered gabbros, and from ~+6 to +15‰ in upper extrusive basalts (Gregory and Taylor, 1981; Alt et al., 1986; Staudigel et al., 1995; Lecuyer and Reynard, 1996). Smart et al. (2021) attribute the negative correlation between $\delta^{18}O$ and $\delta^{44/40}$Ca values in the Bellsbank eclogite xenoliths to the seawater alteration of the eclogite protolith, but higher $\delta^{44/40}$Ca values (>+1.3‰) were attributed to melt extraction. Smart et al. (2021) does acknowledge, however, that these extreme higher $\delta^{44/40}$Ca values could still be a function of extensive hydrothermal alteration on the Archean seafloor. Therefore, it is expected that metasomatism by fluids/melts derived from the lower-most portions of subducted altered oceanic crust could raise the $\delta^{44/40}$Ca value and lower the $\delta^{18}O$ value of the mantle. Therefore, recycled altered lower oceanic crust could produce the negative correlation between $\delta^{18}O$ and $\delta^{44/40}$Ca values observed in the Slave Craton xenoliths. Metasomatism by fluids emanating from altered oceanic crust has also been invoked to generate Slave craton fibrous diamonds (<200 Ma), especially those containing saline fluids (Weiss et al., 2015).

A fourth possibility is metasomatism via a recycled serpentinite component. Serpentinites have distinctively low $\delta^{18}O$ values that range from ~0 to +6‰ (e.g., Wenner and Taylor, 1974; Gregory and Taylor, 1981). However, to date, Ca isotope work on serpentinites is limited. John et al. (2012) report near-mantle to slightly higher than mantle $\delta^{44/40}$Ca values for four obducted high-pressure serpentinites from the Raspas Complex in Ecuador (+0.76 to +1.09‰; n = 4). To our knowledge, there have not been any published studies measuring the Ca isotope composition of seawater-altered abyssal serpentinites. Although it is likely that serpentinites inherit Ca from the oceanic crust protolith, we speculate that seawater-altered serpentinites could incorporate Ca from the ocean, which has a very high $\delta^{44/40}$Ca value (+1.83‰; Fantle and Tipper, 2014). If this is the case, recycled seawater-altered serpentinite could also potentially explain the low $\delta^{18}O$ and high $\delta^{44/40}$Ca values observed in Fig. 5.

5.1.2. Relationships between $\delta^{18}O$ and $\delta^{44/40}$Ca values and major/trace element concentrations in metasomatic minerals

Pairing $\delta^{18}O$ and $\delta^{44/40}$Ca values with major and trace elements and radiogenic tracers in mantle xenoliths is an effective method to identify metasomatic fluids/melts related to subduction (e.g., Hao et al., 2015; Marshall et al., 2017a; Wang et al., 2018; Fitzpayne et al., 2019a). The study by Kilgore et al. (2020) on some of the same mantle xenoliths from the Slave craton as this study (samples with DDM prefix) identified positive correlations between garnet H content and garnet CaO, Na_2O, NiO, Cr_2O_3 concentrations, Cr# (Cr/(Cr + Al)), and La/Lu, Gd/Lu, Sm/Er, and Ce/Yb ratios. The authors attributed the observed correlations to

Table 2
$\delta^{44/40}Ca$ values for mineral separates.

Sample	Average $\delta^{44/40}Ca_{cpx}$ (‰)	2 s.e. (‰)	n	Average $\delta^{44/40}Ca_{grt}$ (‰)	2 s.e. (‰)	n	$\Delta^{44/40}Ca_{cpx\text{-}grt}$ (‰)	2 s.e. (‰)
MX158	0.90	0.10**		1.42	0.10**		0.52	0.14
MX5001	0.88	0.10**		1.00	0.08	3	0.12	0.13
MX5020*								
DDM_149	1.07	0.10**		1.23	0.10**		0.16	0.14
DDM_327	0.99	0.02	2	0.99	0.10**		0.00	0.10
DDM_335	1.01	0.10**		1.10	0.10**		0.09	0.14
DDM_359	1.11	0.10**		1.20	0.10	2	0.09	0.14
DDM_360	0.95	0.10**		1.05	0.10	4	0.10	0.14
DDM_361	1.11	0.10**		1.53	0.10**		0.42	0.14
DDM_367*	0.99	0.10**						
DDM_368	0.99	0.10**		1.09	0.06	3	0.07	0.12
DDM_384*	1.00	0.10**						
Average	1.00			1.18			0.17	
1 s.d.	0.08			0.19			0.17	

* Insufficient garnet for calcium isotope analysis.
** Samples with no replicates analyzed have an uncertainty equal to the 2 s.d. of standards.

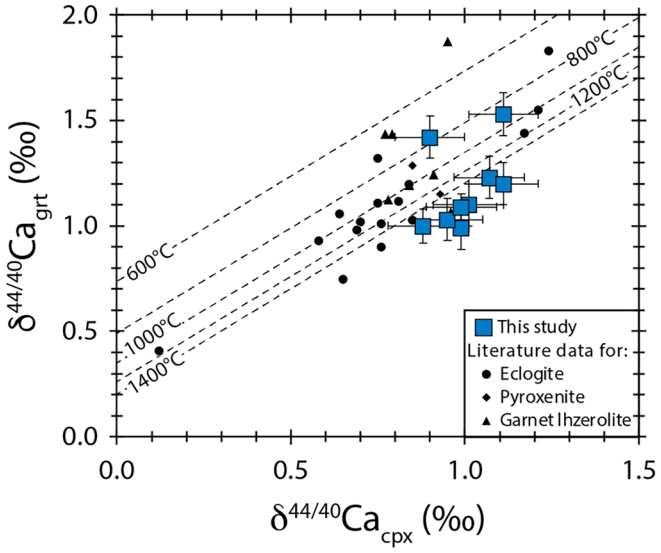

Fig. 4. $\delta^{44/40}Ca_{grt}$ (‰) vs. $\delta^{44/40}Ca_{cpx}$ (‰) values from this study compared to mineral $\delta^{44/40}Ca$ values (‰) of previously published garnet lherzolites (black triangles; Wang et al., 2019; Tappe et al., 2021), pyroxenites (black diamonds; Dai et al., 2020) and eclogites (black circles; Antonelli et al., 2019; Kang et al., 2019; Smart et al., 2021) and equilibrium isotope fractionation for temperatures ranging from 600 °C to 1400 °C (Huang et al., 2019).

metasomatism by a kimberlitic melt that evolved during ascent through the lithosphere. In this study, we document correlations between $\delta^{18}O_{grt}$ and $\delta^{44/40}Ca_{grt}$ values and garnet Na_2O, H_2O, and $(La/Yb)_N$ content (Fig. 7a–f), that suggest samples with non-mantle-like $\delta^{18}O$ and $\delta^{44/40}Ca$ values have trace element signatures that are inherited from a recycled component.

Fig. 7a and d shows correlations between $\delta^{18}O_{grt}$ values and garnet Na_2O concentrations and $\delta^{44/40}Ca_{grt}$ values and garnet Na_2O concentrations. Previous studies have shown that garnets in diamond-bearing eclogites have a higher Na_2O range (0.09–0.22 wt.%) compared to garnets from low-pressure eclogites (0.01–0.06 wt.%), suggesting a link between high Na_2O concentration and pressure (Sobolev and Lavrent'ev, 1971). However, our sample suite displays no correlation between estimated pressure (determined from the Al-in-opx barometer from Brey and Köhler (1990)) and garnet Na_2O concentration. This suggests that garnet Na_2O concentration in the peridotite xenoliths is not primarily a function of pressure. Instead, the variations of Na_2O observed in these garnets are likely related to Na being a fluid-mobile element that concentrates in the ^{16}O-^{44}Ca- enriched melt/fluid that interacted with these samples. The source of the alkalis in the melt can be attributed to subducted altered oceanic crust, as lower oceanic crust gabbros have ~3 wt.% bulk Na_2O, low $\delta^{18}O$ values, and higher $\delta^{44/40}Ca$ values (Gregory and Taylor, 1981; Alt et al., 1986; Staudigel et al., 1995; Bach et al., 2001; Kelley et al., 2003; John et al., 2012; Blättler and Higgins, 2017). This fits well with the model proposed by Weiss et al. (2015) that highly saline fluids derived from a subducting slab are the source of fluid-rich diamonds from the Ekati mine in the Slave Craton.

Additionally, garnet water content increases with decreasing $\delta^{18}O_{grt}$ values (Fig. 7b) and increasing $\delta^{44/40}Ca_{grt}$ values (Fig. 7e). The source of the water in the garnet is likely related to subducted altered oceanic crust. On average, altered basalts and gabbros are significantly enriched in H_2O compared to fresh MORB (e.g., Staudigel, 2017). For example, altered oceanic crust from ODP Hole 1256D have bulk water contents ranging from 0.35 to 2.14 wt.%, significantly higher than in fresh MORB (Shilobreeva et al., 2011). Therefore, fluids/melts derived from altered oceanic crust can lower the $\delta^{18}O_{grt}$ and raise the $\delta^{44/40}Ca_{grt}$ and H content of the surrounding mantle.

Lastly, Fig. 7c shows a negative correlation between garnet $(La/Yb)_N$ ratios and $\delta^{18}O_{grt}$ values. Additionally, Fig. 7f shows a positive correlation between garnet $(La/Yb)_N$ ratios and $\delta^{44/40}Ca_{grt}$ values. High LREE/HREE ratios can be interpreted as reflecting the incorporation of recycled crustal material, although they can also be inherited by interaction with a highly fractionated melt, such as carbonatites, or from LREE-enriched melts, such as OIBs and kimberlites. Therefore, we suggest that the increase in the $(La/Yb)_N$ ratio and the accompanied decrease/increase in the $\delta^{18}O_{grt}/\delta^{44/40}Ca_{grt}$ value, respectively, is derived from a LREE-enriched melt/fluid of subducted seawater-altered oceanic crust.

Many studies have reported and observed negative $\Delta^{18}O_{cpx\text{-}ol}$ fractionations in mantle-sourced rocks and have attributed this signature to metasomatism that preferentially lowers the $\delta^{18}O$ value of the pyroxenes (Gregory and Taylor, 1986; Deines and Haggerty, 2000; Zhang et al., 2000; Orr and Luth, 2000). Both $\Delta^{18}O_{cpx\text{-}ol}$ and $\Delta^{18}O_{grt\text{-}ol}$ values from this study are lower than estimated equilibrium values predicted by theoretical calculations at 900 °C to 1400 °C or observed in experimental studies ($\Delta^{18}O_{cpx\text{-}ol}$ = +0.40‰ to +0.70‰; Chiba et al., 1989; Rosenbaum et al., 1994; Valley, 2003; $\Delta^{18}O_{grt\text{-}ol}$ = +0.50‰ to +0.90‰; Zheng, 1993). Evidence to support that non-equilibrium $\Delta^{18}O$ and $\Delta^{44/40}Ca$ values are related to metasomatism is shown in Fig. 8. Here, the same negative correlations between trace element indices of metasomatism in Fig. 7 coupled with the $\delta^{18}O_{grt}$ and $\delta^{44/40}Ca_{grt}$ values are also observed with the $\Delta^{18}O_{grt\text{-}ol}$, $\Delta^{18}O_{grt\text{-}cpx}$, and $\Delta^{44/40}Ca_{grt\text{-}cpx}$ values. The negative correlations between garnet Na_2O, H_2O, and $(La/Yb)_N$ and $\Delta^{18}O_{grt\text{-}ol}$ show that the least metasomatized samples have positive $\Delta^{18}O_{grt\text{-}ol}$ (Fig. 8a–c) and $\Delta^{18}O_{grt\text{-}cpx}$ (Fig. 8d–f). These values are closer to equilibrium fractionation estimates at temperatures ranging from

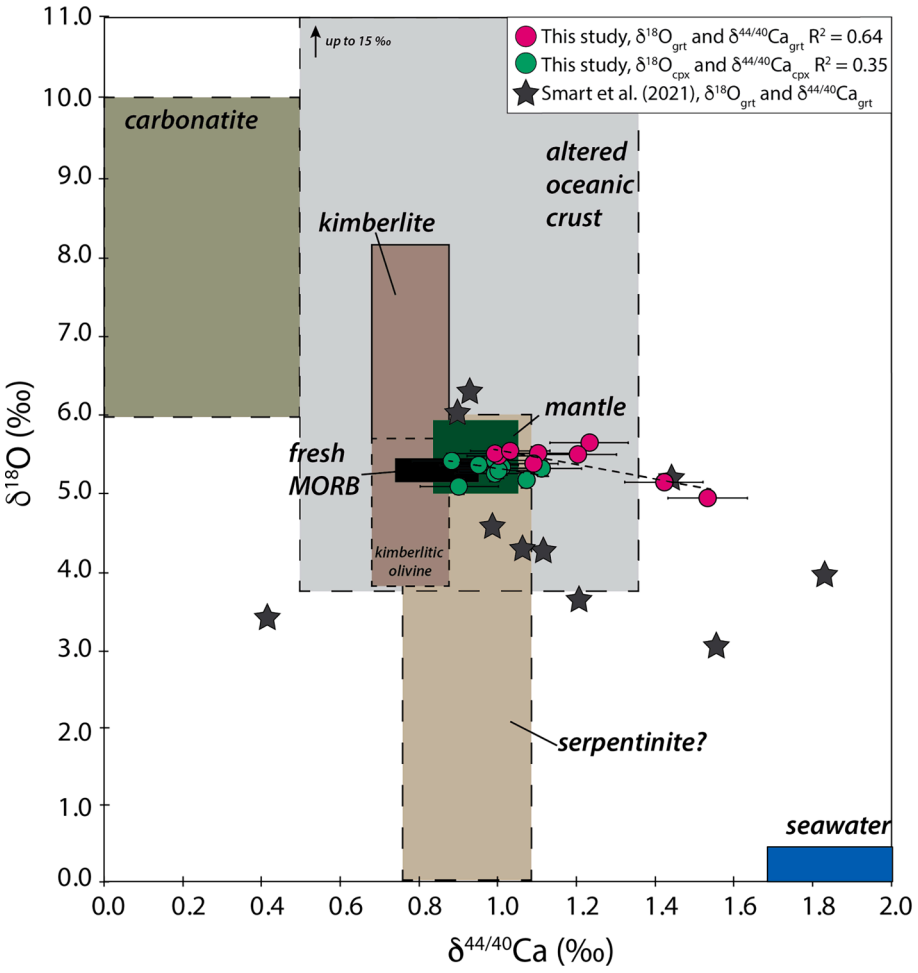

Fig. 5. $\delta^{18}O_{grt}$ (‰) versus $\delta^{44/40}Ca_{grt}$ (‰) of from this study (pink circles) and $\delta^{18}O_{cpx}$ (‰) versus $\delta^{44/40}Ca_{grt}$ (‰) from this study (green circles) and $\delta^{18}O_{grt}$ (‰) versus $\delta^{44/40}Ca_{grt}$ (‰) of garnet minerals from Bellsbank eclogites from the Kaapvaal Craton from Smart et al. (2021). The typical range for $\delta^{18}O$ and $\delta^{44/40}Ca$ values (‰) of the following reservoirs: altered oceanic crust (light gray box; John et al., 2012; Blättler and Higgins, 2017; Kelley et al., 2003; Bach et al., 2001), mantle (green box; Mattey et al., 1994; Chen et al., 2019), fresh MORB (black box; Zhu et al., 2018; Harmon and Hoefs, 1995), erupted kimberlites (brown box; Price et al., 2000; Fedortchuk and Canil, 2004; Wilson et al., 2007; Antonelli et al., 2023), carbonatite (olive green box; Horstmann and Verwoerd, 1997; Amsellem et al., 2020) and seawater (blue box; Fantle and Tipper, 2014), serpentinites (Wenner and Taylor, 1974; John et al., 2012).

Table 3
δD values of kelyphitic rims.

Sample	Average δD (‰)	1 s.d. (‰)
MX158	−106	3.1
MX5001	−118	0.7
MX5020	−136	2.8
DDM_149*		
DDM_327*		
DDM_335	−131	2.1
DDM_359	−128	0.0
DDM_360	−125	2.8
DDM_361	−137	0.7
DDM_367	−145	0.7
DDM_368	−129	0.7
DDM_384	−108	2.1

* Insufficient kelyphitic rim material for hydrogen isotope analysis.

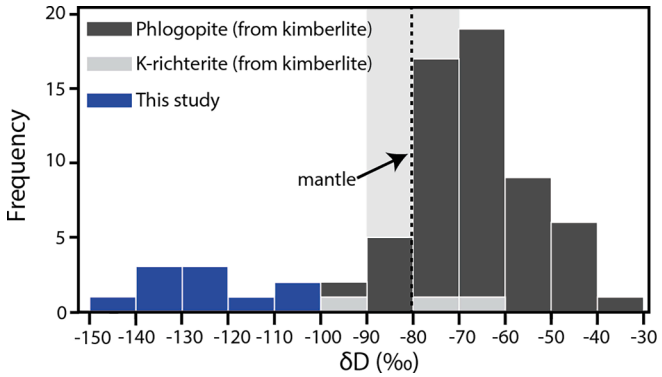

Fig. 6. Kelyphitic rims δD value (‰) from this study compared to phlogopite δD values (‰) from Sheppard and Epstein (1970), Kuroda et al. (1975, 1977), Sheppard and Dawson (1975), Boettcher and O'Neil (1980), and Banerjee et al. (2018) and k-richterite δD values from Kuroda et al. (1975) and Banerjee et al. (2018).

1200 to 1400 °C. The more metasomatized samples (with higher garnet Na_2O, H_2O, and $(La/Yb)_N$) have lower $\Delta^{18}O_{grt\text{-}ol}$ and $\Delta^{18}O_{grt\text{-}cpx}$ values that are the furthest from isotopic equilibrium. Therefore, we suggest that metasomatism by a melt/fluid with low $\delta^{18}O$ preferentially lowered the garnet oxygen isotope composition relative to olivine, resulting in the observed non-equilibrium $\Delta^{18}O_{grt\text{-}ol}$ values. Alternatively, the subduction-derived metasomatism was modal, leading to the growth of new garnet and clinopyroxene, or cryptic, resulting in the growth and overprinting of new garnet and clinopyroxene.

Only a few studies have measured $\delta^{18}O$ in both olivine and garnet in

Table 4
Sm-Nd isotope systematics for mineral separates.

Sample	Mineral	Sm (ppm)	Nd (ppm)	$^{147}Sm/^{144}Nd$	2 s.d.	$^{143}Nd/^{144}Nd$	2 s.d.	ε_{Nd}
MX158	cpx	1.54	13.7	0.0680	0.0012	0.512170	0.000015	−9.2
	grt	0.63	1.4	0.2721	0.0012	0.511793	0.000015	−16.5
DDM_327	grt	0.63	0.97	0.3924	0.0012	0.512687	0.000015	0.9
DDM_361	cpx	0.99	5.87	0.1024	0.0012	0.512587	0.000015	−1.0
DDM_367	cpx	1.18	8.68	0.0822	0.0012	0.512552	0.000015	−1.7
	grt	0.85	1.85	0.2772	0.0012	0.512616	0.000015	−0.4
DDM_368	cpx	0.25	1.75	0.0867	0.0012	0.512515	0.000015	−2.4
	grt	4.55	8.83	0.3116	0.0012	0.512536	0.000015	−2.0

Table 5
Model Sm-Nd depletion ages for whole rock xenoliths.

Sample	Calculated WR $^{147}Sm/^{144}Nd$	Calculated WR $^{143}Nd/^{144}Nd$	Sm-Nd model age BSE (Ma)*	Sm-Nd model age DM (Ma)*
MX158	0.0730	0.512150	315	698
DDM_361**	–-	–-	35	70
DDM_367	0.0904	0.512560	67	194
DDM_368**	–-	–-	79	161

* Ages are calculated relative to bulk silicate earth values ($^{143}Nd/^{144}Nd$ = 0.512638; Sm/Nd = 0.325) & depleted mantle ($^{143}Nd/^{144}Nd$ = 0.51326; Sm/Nd = 0.435) after Workman and Hart (2005).

** Model age is calculated from clinopyroxene Sm/Nd isotope compositions listed in Table 4 either due to lack of modal abundance data or because there are no Sm/Nd isotope data for garnet.

the same mantle peridotite xenoliths, with even a smaller subset of those samples that have measured clinopyroxene as well. These studies report $\Delta^{18}O_{grt\text{-}ol}$ fractionations that range from −0.54‰ to +0.70‰ with an average of +0.05 ± 0.26‰ (1σ; n = 27; Ionov et al., 1994; Mattey et al., 1994; Lowry et al., 1999; Deines and Haggerty, 2000; Rehfeldt et al., 2008; Wang et al., 2011; Fitzpayne et al., 2019a; Lebedeva et al., 2020); and $\Delta^{18}O_{grt\text{-}cpx}$ values that range from −0.88‰ to + 1.33‰ with an average of −0.12 ± 0.55‰ (1σ; n = 13; Ionov et al., 1994; Lowry et al., 1999; Zhang et al., 1999; Deines and Haggerty, 2000; Rehfeldt et al., 2008; Wang et al., 2011; Fitzpayne et al., 2019a; Lebedeva et al., 2020). These values are, for the most part, also lower than predicted for equilibrium fractionation between garnet and olivine and garnet and clinopyroxene. However, only two of these studies (Wang et al., 2011; Fitzpayne et al., 2019) corrected the garnet $\delta^{18}O$ value for the Cr-effect documented by Wang et al. (2011). If the data from these previous studies are corrected for the Cr-effect using the reported Cr_2O_3 concentrations, then the average $\Delta^{18}O_{grt\text{-}ol}$ value of these eight studies (+0.27 ± 0.21‰; 1σ; n = 27) and the $\Delta^{18}O_{grt\text{-}cpx}$ value (−0.02 ± 0.53‰;

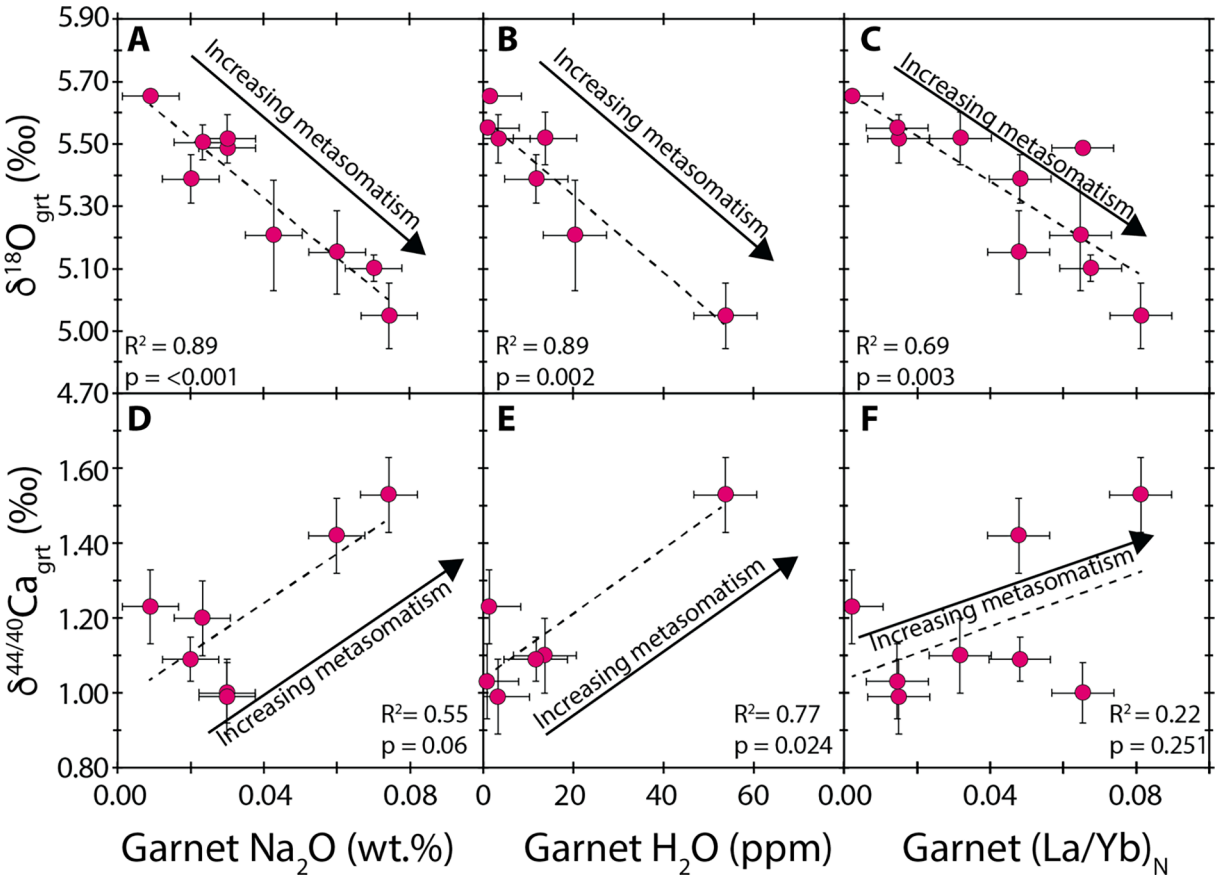

Fig. 7. $\delta^{18}O_{grt}$ (‰) on the top and $\delta^{44/40}Ca_{grt}$ (‰) on the bottom are plotted vs. garnet Na_2O content (wt.%) (in a and d; Creighton et al., 2010; Kilgore et al., 2020), water content (ppm) (in b and e; Kilgore et al., 2020)), and chondrite-normalized (McDonough and Sun, 1995) rare earth element ratios ($(La/Yb)_N$ in c and f; Creighton et al., 2010; Kilgore et al., 2020)).

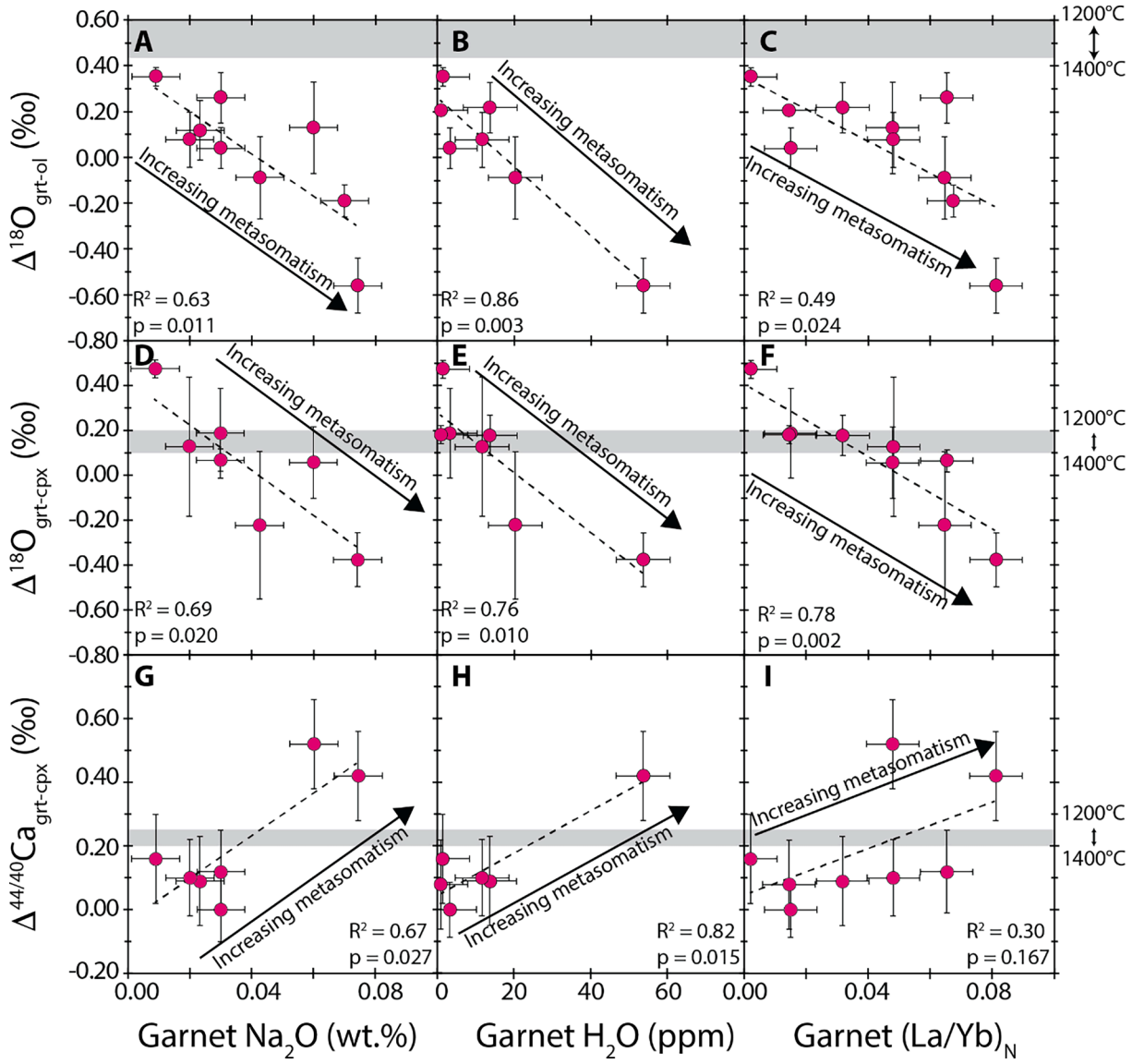

Fig. 8. $\Delta^{18}O_{grt\text{-}ol}$ (‰) on the top, $\Delta^{18}O_{grt\text{-}cpx}$ (‰) in the middle, and $\Delta^{44/40}Ca_{grt\text{-}cpx}$ (‰) on the bottom are plotted vs. garnet Na_2O content (wt.%) (in a, d, and g; Creighton et al., 2010; Kilgore et al., 2020), water content (ppm) (in b, e, and h; Kilgore et al., 2020)), and chondrite-normalized (McDonough and Sun, 1995) rare earth element ratios ($(La/Yb)_N$ in c, f, and i; Creighton et al., 2010; Kilgore et al., 2020)). Equilibrium fractionation factors for temperatures ranging from 1200 °C to 1400 °C are shown on the right.

1σ; n = 13) is increased, but is still lower than predicted equilibrium fractionation at temperatures from 900 to 1400 °C ($\Delta^{18}O_{grt\text{-}ol}$ = +0.50‰ to +0.90‰; $\Delta^{18}O_{grt\text{-}cpx}$ = 0.00‰ to +0.20‰; Zheng, 1993). Although not all of these studies directly link low $\Delta^{18}O_{grt\text{-}ol}$ or $\Delta^{18}O_{grt\text{-}cpx}$ to evidence of metasomatism (as many reporting low $\Delta^{18}O_{cpx\text{-}ol}$ values have done), many of these studies have identified mantle metasomatism in sample suites where non-equilibrium $\Delta^{18}O_{grt\text{-}ol}$ and $\Delta^{18}O_{grt\text{-}cpx}$ values are reported (Deines and Haggerty, 2000; Rehfeldt et al., 2008; Wang et al., 2011; Fitzpayne et al., 2019; Lebedeva et al., 2020).

Studies on mineral Ca isotope fractionation in mantle peridotites has largely focused on clinopyroxene and orthopyroxene (avg. $\Delta^{44/40}Ca_{opx\text{-}cpx}$ = +0.25 ± 0.45‰; 1σ; n = 41; Huang et al., 2010; Kang et al., 2016; Zhao et al., 2017; Chen et al., 2018; Chen et al., 2019; Kang et al., 2020). In contrast, studies of Ca isotope fractionation between garnet and clinopyroxene in peridotites are limited, with only two studies reporting values averaging +0.48 ± 0.28‰ (1σ; n = 7; Wang et al., 2019; Tappe et al., 2021). For eclogites and pyroxenites, average $\Delta^{44/40}Ca_{grt\text{-}cpx}$ values are reported as +0.30 ± 0.11‰ (1σ; n = 15; Kang et al., 2019; Smart et al., 2021) and +0.33 ± 0.16‰ (1σ; n = 2; Dai et al., 2020), respectively. Garnet preferentially incorporates the heavier ^{44}Ca isotope relative to ^{40}Ca due to shorter Ca—O bond lengths than clinopyroxene (Magna et al., 2015). This results in theoretical equilibrium fractionation factors, $\Delta^{44/40}Ca_{grt\text{-}cpx}$ values, to range from +0.20 to +0.25‰ at temperatures 1200–1400 °C (Antonelli et al., 2019; Huang et al., 2019). Samples in this study generally cluster above and below predicted equilibrium fractionation, with errors falling within the predicted Ca isotope fractionation between garnet – clinopyroxene (between +0.20 and +0.25‰). The exceptions are samples MX158 and DDM_327. Notably, with the exception of these samples, $\delta^{44/40}Ca$ values of clinopyroxene and garnet are well correlated (Fig. 4), suggesting equilibrium.

Fig. 8g–i shows that samples with higher $\Delta^{44/40}Ca_{grt\text{-}cpx}$ values have higher garnet Na_2O and H_2O concentrations, and higher $(La/Yb)_N$ ratios than samples with lower $\Delta^{44/40}Ca_{grt\text{-}cpx}$ values suggesting that the subduction derived metasomatism played a role in the variations of the $\Delta^{44/40}Ca_{grt\text{-}cpx}$ values. It is noted that the variations we observed in the $\Delta^{44/40}Ca_{grt\text{-}cpx}$ values are much more limited than large fractionations ($\Delta^{44/40}Ca_{grt\text{-}cpx}$ values up to +2‰) that are recorded by granulite facies lower crustal xenoliths, even some from the A154N kimberlite from the Diavik

Diamond Mine (Antonelli et al., 2019). Larger $\Delta^{44/40}$Ca values (>+1‰) are attributed to kinetic Ca isotope effects and are found to correlate with Mg# (Zhao et al., 2017; Antonelli et al., 2019; Kang et al., 2020) due to the compositional effect on kinetic Ca isotope fractionation that occurs during melt-peridotite interaction. To disentangle equilibrium effects from any kinetic and compositional effects, we plotted the $\Delta^{44/40}Ca_{grt\text{-}cpx}$ vs. garnet and whole rock Mg#, revealing no significant correlations (Fig. S6). This suggests the variations observed in the $\Delta^{44/40}Ca_{grt\text{-}cpx}$ are also associated with the subduction-derived metasomatism.

5.1.3. δD evidence for a recycled crustal component

This study investigated the hydrogen isotope composition of whole kelyphitic rims rather than individual grains of phlogopite due to the fine-grained nature of the rims. The δD value of the rims (−126 ± 13‰) is very different from the δD value reported for phlogopite from kimberlites worldwide (δD = −65 ± 12‰; Fig. 6; Sheppard and Epstein, 1970; Sheppard and Dawson, 1975; Kuroda et al., 1975, 1977; Boettcher and O'Neil, 1980; Banerjee et al., 2018). One possible explanation for the low δD of the kelyphitic rims is the interaction with subduction-related fluids. Recent studies have found that subduction processes can fractionate the D/H ratio of Earth's reservoirs (Shaw et al., 2008; Walowski et al., 2015). Water is carried into Earth's mantle at subduction zones via hydrous mineral phases in subducting lithospheric plates. A fraction of this water is released during subduction, leading to the generation of arc volcanism. Arc-related magmatic melt inclusions have high δD values (e.g., −55‰ to −12‰ from the Marianas arc; Shaw et al., 2008; and −66‰ to −33‰ from the Cascadian arc; Walowski et al., 2015). The water released from the subducting slab into the overlying mantle wedge is enriched in D, forming a D-depleted slab. This suggests that ocean island basalts (OIBs) that contain recycled slab components should be characterized by low δD values. This is observed in melt inclusions from Hawaii, which have δD_{avg} = −121 ± 35‰ (1σ; n = 19; Hauri, 2002). The low δD values recorded in the kelyphitic rims from the Slave craton are consistent with fluids derived from deeply subducted slab residues that have lost some of their water during subduction-induced dehydration.

Overall, several lines of evidence show that these Slave craton xenoliths have been metasomatized by a melt/fluid characterized by elevated $\delta^{44/40}$Ca values and low δ^{18}O and δD values. This metasomatism enriched samples in H_2O, LREEs, and Na. We argue the most likely origin of this fluid/melt is subducted lower altered oceanic crust, although we cannot rule out serpentinites given the lack of published Ca isotope data on serpentinites.

5.2. Timing of subduction-related metasomatism: O isotope diffusion and Nd isotopes

Nd isotopes can provide general constraints on the timing of the observed subduction-related metasomatism and whether it was associated with the initial stabilization of the Slave subcontinental lithospheric mantle during the Archean or whether it occurred more recently during the Proterozoic or Phanerozoic. Calculated Sm-Nd whole rock model ages relative to bulk silicate earth (BSE) and depleted mantle (DM) values (Workman and Hart, 2005) are listed in Table 5. Given that these samples' calculated whole rock Sm-Nd isotope ratios are very similar to each sample's respective clinopyroxene Sm-Nd composition, model ages were calculated for samples DDM_361 and DDM_368 based on the clinopyroxene Sm-Nd isotope ratios to give a rough age estimate (Table 5). Sm-Nd BSE and DM model ages (Table 5) indicate a Phanerozoic age for the metasomatism with the exception of a DM model age of sample MX158 (698 Ma; Fig. 9). This confirms that the subduction-derived metasomatism occurred more recently (within the last ~700 Ma) and did not coincide with the initial stabilization of the craton during the Archean.

Despite the Sm-Nd isotope system's utility in providing age constraints, the results are affected by the low abundance of Sm and Nd in depleted peridotites, making them prone to metasomatic overprinting, including from the host kimberlite (i.e., Schmidberger et al., 2007). The $^{143}Nd/^{144}Nd$ in both clinopyroxene and garnet from samples MX158, DDM_327, DDM_361, DDM_367, and DDM_368 overlap with the kimberlite Nd isotope composition of the A154 pipe ($^{143}Nd/^{144}Nd$ = 0.512500; Tappe et al., 2013; Fig. 10). The narrow range in $^{143}Nd/^{144}Nd$ over a large range of $^{147}Sm/^{144}Nd$ observed in minerals from this sample suite is similar to the range reported for a suite of deep peridotite samples from the Diavik mine (Aulbach et al., 2013; Fig. 10), suggesting that metasomatism may be related to the kimberlite magmatism as suggested by Kilgore et al. (2020).

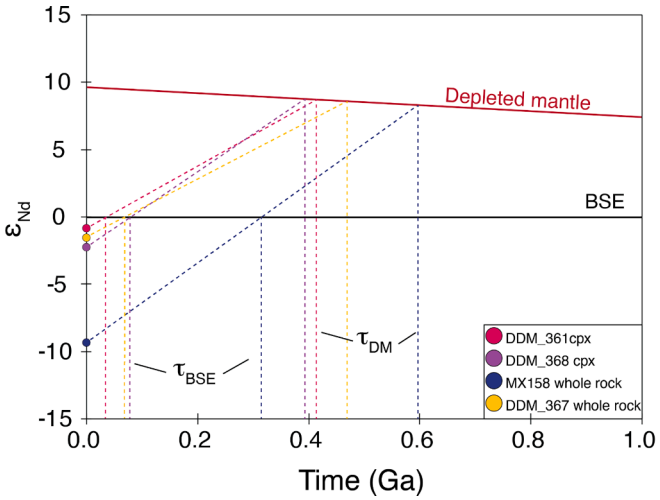

Fig. 9. ε_{Nd} vs. time for calculated whole rock samples and clinopyroxene to show Sm-Nd model ages compared to BSE (τ_{BSE}) and DM (τ_{DM}). DM and BSE evolution curves are shown as red and green lines, respectively (Workman and Hart, 2005).

Oxygen isotope diffusion modeling can provide tighter constraints on when the subduction-related metasomatism occurred as inter-mineral oxygen isotope disequilibrium can be preserved in the mantle at temperature-dependent diffusive timescales. Diffusion modeling was performed for the lherzolites in this study using the equation of Crank (1979), following several recent approaches (Perkins et al., 2006; Hao et al., 2015; Fitzpayne et al., 2019a):

$$\delta^{18}O(t) = \delta^{18}O_{eqm} + (\delta^{18}O_{measured} - \delta^{18}O_{eqm}) \times \mathrm{erf}\left(\frac{r}{2\sqrt{Dt}}\right),$$

where $\delta^{18}O(t)$ is the oxygen isotope composition at time t, $\delta^{18}O_{eqm}$ is the expected equilibrium oxygen isotope composition of the mineral at temperature T, $\delta^{18}O_{measured}$ is the measured oxygen isotope composition of the mineral (Table 1), r is the radius of the mineral, and D is the mineral's diffusion coefficient at temperature T.

The equilibration temperature for each sample is taken from Brey and Köhler temperatures published in previous studies (Creighton et al., 2010; Kilgore et al., 2020), and the average radius of clinopyroxene and garnet grains are obtained from thin section (Supplemental Table S.1). Oxygen isotope diffusion modeling was only conducted on samples with grain size measurements (MX158, DDM_149, DDM_329, DDM_335, DDM_361, and DDM_367). It is assumed that the coexisting olivine provides the equilibrium conditions of the local ambient mantle, given the similarity between measured olivine values (+5.02 to +5.48‰ Table 1; Fig. 2a) and published values for lithospheric mantle olivine (+5.2 ± 0.3‰; Mattey et al. 1994). The expected equilibrium $\delta^{18}O$ values for both clinopyroxene and garnet ($\delta^{18}O_{eqm}$) were calculated using fractionation factors from Zheng (1999) and Valley (2003). Diffusion coefficients for clinopyroxene were calculated using data from Ingrin et al. (2001) at an average equilibration temperature of 1250 °C.

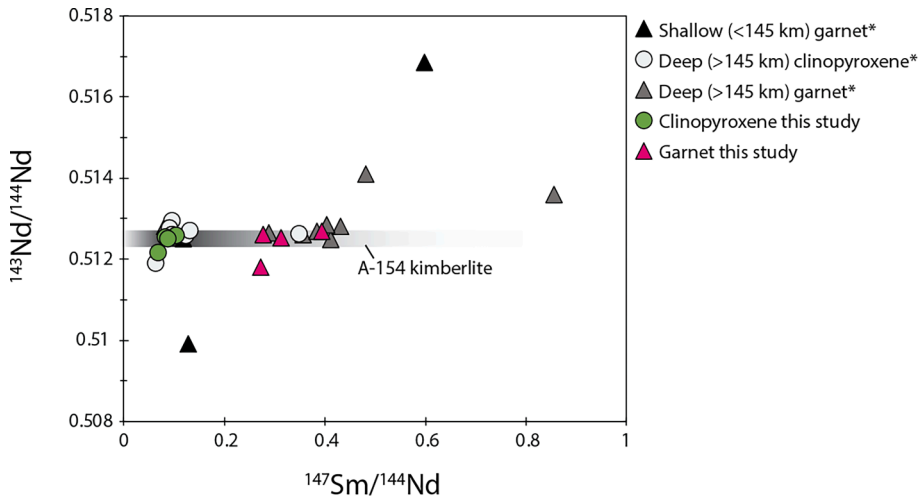

Fig. 10. Plot of $^{147}Sm/^{144}Nd$ vs. $^{143}Nd/^{144}Nd$ for clinopyroxene (green circles) and garnet (pink triangles) minerals from xenoliths from this study. Also shown are compositions of clinopyroxenes and garnets from xenoliths from the A154 kimberlite pipe that equilibrated at shallower depths from Aulbach et al. (2013) and the composition of the A154 kimberlite that brought the samples from this study and Aulbach et al. (2013) to the surface (Tappe et al., 2013).

Diffusion coefficients for garnet minerals were extrapolated from Coughlan's (1990) data at a temperature of 1250 °C. At these high temperatures (1200–1350 °C), clinopyroxene and garnet can only retain non-equilibrium $\delta^{18}O$ values for times scales of 10,000–100,000 years (Fig. 11; depending on the radius, measured composition, and equilibration temperature). These short time scales indicate that the metasomatism recorded by the mineral-scale oxygen isotope disequilibrium had to occur shortly before or during entrainment by the kimberlite host at 55 Ma (Graham et al., 1999; Creaser et al., 2004).

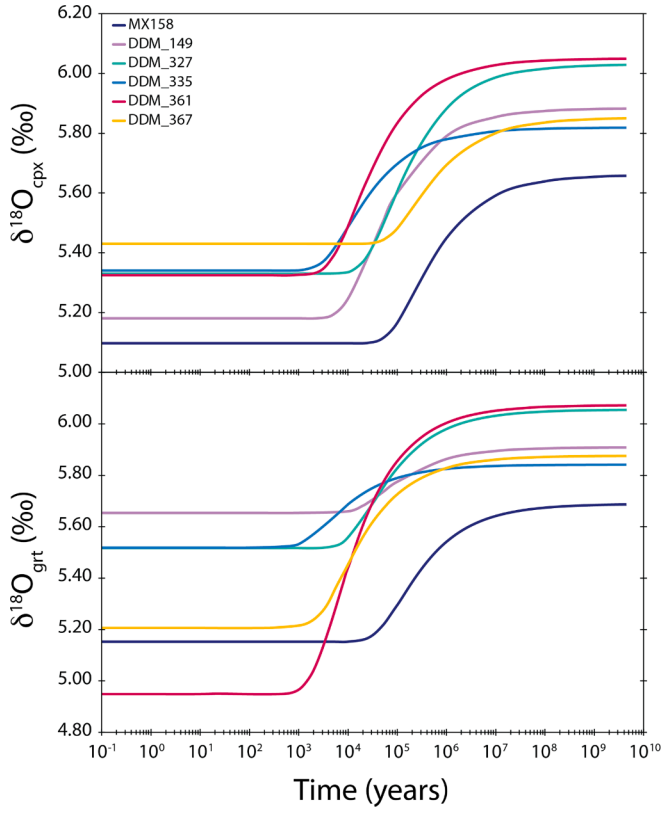

Fig. 11. $\delta^{18}O$ (‰) vs. time (years) for clinopyroxene (top panel) and garnet (bottom panel) samples from this study, showing change in $\delta^{18}O$ value over time due to diffusion within clinopyroxene and garnet, triggered by progressive isotopic equilibration between clinopyroxene/garnet and local ambient mantle; see text for details.

5.2.1. Subduction-derived metasomatism related to kimberlite melt?

Given the oxygen isotope diffusion modeling and the observed inter-mineral disequilibria, the subduction-related metasomatism we have noted has to have been nearly contemporaneous with kimberlite eruption since the disequilibria can be maintained for $<10^5$ years. This requires a subduction-related metasomatism event nearly the same age as the 55.4 Ma kimberlite eruption, or possibly that the kimberlite itself acted as the metasomatic agent. We propose three hypotheses that link the observed subduction metasomatism and kimberlite volcanism to explain the contemporaneous nature of the metasomatism and kimberlite volcanism.

The near contemporaneous metasomatism and kimberlite eruption could be related to (1) the kimberlite melt triggering the movement of subduction-derived fluids that were stabilized in the SCLM during flat-slab subduction in the Mesozoic. It has been noted that flat-slab subduction, commonly associated with the Laramide orogeny in the southwestern United States, was in place as far north as ~60°N (Currie and Beaumont, 2011), although other geodynamic models (i.e., Liu et al., 2010) argue Laramide low angle subduction didn't extend beyond the Wyoming craton (~48°N). Despite this, a decrease in the angle of the subducting slab can cause the subducted oceanic plate to come into contact with the base of the overlying SCLM, cooling the SCLM (Smith, 2010). Additionally, as the oceanic plate dehydrates, it releases hydrous fluids and melts, metasomatizing the overlying SCLM (Lee, 2005). The cooler temperatures allow hydrous mineral formation and stabilization in the hydrated SCLM (Humphreys et al., 2003). The percolation and intrusion of the kimberlitic melt at 55 Ma could have triggered the movement of these subduction-derived fluids that were already present in the SCLM, providing an explanation for why kimberlite volcanism and the metasomatism occurred within 100,000 years of each other.

Alternatively, (2) this subduction-derived fluid could have been a precursor fluid that triggered kimberlite emplacement. Kamenetsky et al. (2013) and references therein have proposed parental kimberlite liquid was a Si-poor, Ca—Mg carbonate-rich fluid, enriched in alkali elements, lithophile trace elements, P, Cl, and S. Some studies have concluded from geochemical and experimental data that the Cl-bearing carbonate precursors of kimberlites could be the products of saline fluids metasomatizing peridotites in the surrounding lithospheric mantle (Navon et al., 2008; Klein-BenDavid et al., 2009; Safonov et al., 2009; Weiss et al., 2009). The subduction-derived, Na-rich fluid we infer to have metasomatized the Slave craton xenoliths has characteristics that

are similar to the saline fluids proposed to have produced fluid-rich diamonds from the Ekati mine in the Slave craton (Weiss et al., 2015), with the majority of these diamonds having formed within 1 Ma of kimberlite volcanism. Additionally, Tappe et al. (2013) identified that Cretaceous and Eocene-aged kimberlites from the Lac de Gras area exhibit extreme Nd-Hf isotope decoupling compared to kimberlites globally and attribute this trend to an ancient, subducted component in the kimberlite source region. They argue that the incorporation of this material was due to mantle return flow related to complex subduction along the western margin of North America during the Cretaceous. Active subduction zones, from at least 170 Ma to ~70–50 Ma (Shephard et al., 2014), were a key feature of the complex tectonic setting of western North America and the Arctic, providing several options for the fluid source in the ideal time window to allow for metasomatism of the xenoliths. Therefore, the initiation of kimberlite volcanism by a subduction-related fluid can explain the metasomatism coinciding with kimberlite volcanism.

Lastly, (3) the kimberlite melt itself could act as the metasomatizing agent, provided the kimberlite melt is derived from a subducted source. There are many proposed models for kimberlite genesis, such as mantle plumes (i.e., Crough et al., 1980), continental extension (i.e., Phipps, 1988), melts originating from the mantle transition zone and deeper (i.e., Ringwood et al., 1992; Torsvik et al., 2010), and lithospheric subduction (i.e., Currie and Beaumont, 2011). The origin of kimberlite sources is unclear, and whether subducted components are involved is still debated today. Ultimately, the oxygen and calcium isotope compositions are not well-constrained for kimberlite materials. The O isotope composition of minerals (typically micas, carbonates, serpentines, sulfides) in kimberlite magmas show a wide range of $\delta^{18}O$ values from +1.2‰ to +17.4‰, with an average $\delta^{18}O = +8.7 \pm 3.2$‰ (1σ; Price et al., 2000; Fedortchuk and Canil, 2004; Wilson et al., 2007). Although the average kimberlite $\delta^{18}O$ value is higher than typical mantle values, Price et al. (2000) state that a $\delta^{18}O$ range of +6.2 to +8.2‰ lies within the range established for mica and serpentine found in kimberlite groundmass and is consistent with derivation from a mantle source. Studies attribute the higher $\delta^{18}O$ values (>+8.2‰) observed in carbonate minerals in the kimberlite groundmass to secondary alteration from meteoric water post-eruption. Only a handful of studies (Guiliani et al., 2019; Xu et al., 2021) have analyzed the oxygen isotope composition of olivine xenocrysts, including cores and rims, in kimberlites to constrain the starting composition of kimberlites. Guiliani et al. (2019) found that the $\delta^{18}O$ values of different olivine zones do not deviate from typical mantle olivine values of $+5.2 \pm 0.3$ (Mattey et al., 1994), which suggests the source of kimberlite magmas are not isotopically distinct from the surrounding mantle. However, Xu et al. (2021) identified kimberlite-hosted olivine xenocryst cores from the Kaapvaal Craton in South Africa and the Rae Craton in Canada with lower than mantle $\delta^{18}O$ values (avg. $= +4.11 \pm 0.28$‰; 1σ; n = 11). They attributed these low $\delta^{18}O$ values and the positive correlations with olivine Mg# to the assimilation of SCLM wall rocks, which have lower-than-average $\delta^{18}O$ values. However, they also suggest that the low $\delta^{18}O$ values in the cores of olivine could originate from the proto-kimberlite melts derived from a low $\delta^{18}O$ mantle region with a recycled crustal source. To our knowledge, Ca isotopes have only been measured on South African kimberlites, with values ranging from +0.68‰ to +1.27‰ with an average of $+0.81 \pm 0.11$‰ (1σ; n = 25; Tappe et al., 2021; Antonelli et al., 2023), so the true Ca isotope range of kimberlites worldwide is not well established. In summary, existing data indicate that low-$\delta^{18}O$ components may be present in kimberlite source, while the evidence for calcium remains unclear. Therefore, kimberlite metasomatism cannot be ruled out, even though kimberlites that have reached the surface generally have higher oxygen and lower calcium isotope compositions than the mantle (light brown box; Fig. 5; Price et al., 2000; Fedortchuk and Canil, 2004; Wilson et al., 2007; Antonelli et al., 2023).

There is experimental and petrographic evidence that kimberlites interact and assimilate with the lithospheric mantle material on their way to the surface and that their chemical composition changes from source to surface (i.e., Russell et al., 2012; Mitchell, 2013; Soltys et al., 2016; Sharygin et al., 2017). More recently, there has been radiogenic isotope evidence that kimberlites evolve and interact with the surrounding mantle material during ascent (Fitzpayne et al., 2019b). Therefore, if the stable isotope composition of the kimberlite source magma is different from the stable isotope composition of the ambient SCLM, the kimberlite magma could evolve to become more mantle-like during ascent and interaction with the ambient mantle. By this logic, deeper-derived mantle xenoliths, as in this study, will retain the isotope signature of the proto-kimberlite melt, and shallower-derived mantle xenoliths will retain the isotope signature of the evolved kimberlite melt that is in isotope equilibrium with the SCLM. Therefore, the isotope composition of clinopyroxene and garnet minerals in the xenoliths from this study could be representative of the stable isotope composition of the proto-kimberlite melt, as these xenoliths equilibrated at depths associated with kimberlite genesis. Therefore, it is possible that the kimberlite source magma could have a low $\delta^{18}O$ and high $\delta^{44/40}Ca$ that could be associated with the subduction of seawater-altered oceanic crust. A caveat to this hypothesis is the study by Zou et al. (2024), which reports that $\delta^{44/40}Ca$ values in melts are minimally modified during transport from depth to the surface when compared to more significant changes observed in other major element stable isotopes, such as Fe and Mg. Further investigation is needed to determine if similar constraints apply to kimberlite magmas.

Kimberlite metasomatism is commonly characterized by Ti enrichment in garnets (i.e., Dongre et al., 2016). Kimberlites from the Lac de Gras area in the central Slave craton have an average TiO_2 concentration of ~0.64 wt.% (Tappe et al., 2013). Therefore, if kimberlites were the metasomatizing agent, we would expect correlations between the $\delta^{18}O$ or $\delta^{44/40}Ca$ and the Ti concentration in garnets or enrichment in high field strength elements relative to LREEs, which are not observed (Fig. S.7), potentially because the A154 pipe that hosted the xenoliths in this study is found to be Ti-depleted (Aulbach et al., 2013; Kilgore et al., 2020) or simply, because the kimberlite was not the metasomatizing agent.

We prefer models (2) and (3) to explain the observed deviations in O, Ca, and H isotopes from the typical mantle and the associated correlations with geochemical tracers of subduction. Ultimately, how or whether the subduction-related metasomatism recorded in the Slave craton mantle xenoliths reported in this study is related to kimberlite emplacement is unclear and cannot be answered with this dataset.

6. Broader geochemical significance and conclusions

The combined isotope data ($\delta^{18}O$, $\delta^{44/40}Ca$, and δD) from this study indicate metasomatism in mantle peridotites from the Slave Craton, despite their resemblance to accepted mantle ranges. Our findings emphasize the importance of subtle variations within the mantle, as they are discernible due to low analytical uncertainty, suggesting that even minor deviations can signal significant processes.

Clinopyroxene and garnet $\delta^{18}O$ values correlate with their respective $\delta^{44/40}Ca$ values, which extend beyond reported mantle ranges to low $\delta^{18}O$ and high $\delta^{44/40}Ca$. Coupled low $\delta^{18}O$ values and high $\delta^{44/40}Ca$ values are attributed to the variable incorporation of altered oceanic crust-derived fluids in the SCLM. This is consistent with negative δD values of phlogopite-bearing kelyphitic rims measured in some samples. Additionally, garnet minerals exhibit major and trace element correlations (Na_2O content, H_2O content, and $(La/Yb)_N$) with $\delta^{18}O_{grt}$ and $\delta^{44/40}Ca_{grt}$ values. These lines of evidence indicate that these deeply entrained mantle xenoliths record the stable isotope and chemical composition of a melt or fluid derived from subducted altered oceanic crust.

Clinopyroxene and garnet minerals are often out of O and Ca isotope equilibrium with each other and out of O isotope equilibrium with coexisting olivine. These variations in observed mineral–mineral oxygen

and calcium isotope fractionation likely result from metasomatism, as the $\Delta^{18}O_{grt\text{-}olv}$, $\Delta^{18}O_{grt\text{-}cpx}$, and $\Delta^{44/40}Ca_{grt\text{-}cpx}$ all correlate with the same indices of metasomatism, garnet Na_2O content, garnet H_2O content, and the garnet $(La/Yb)_N$. This suggests that some minerals, particularly garnet, may be more affected by metasomatic processes than others, leading to isotopic disequilibrium between minerals. Our method offers a new perspective on why more than 50% of mantle peridotites exhibit lower than expected oxygen isotope equilibrium fractionation. These samples' high equilibration temperatures (>1200 °C) reduce the diffusion timescales on which clinopyroxene and garnet minerals maintain oxygen isotope disequilibrium. Diffusion modeling constrains the timing of metasomatism to within 10,000 to 100,000 years before kimberlite entrainment.

This recycled component was likely incorporated in the SCLM during the Mesozoic subduction of oceanic lithosphere beneath the North American continental lithospheric mantle. How this metasomatic fluid is related to kimberlite emplacement is unclear. However, the temporal juxtaposition of metasomatism and kimberlite eruption suggests either that kimberlite melts triggered remobilization of subduction-derived components in the SCLM, that the subduction-derived fluids/melt responsible for metasomatism were precursors to kimberlitic melts, or that the kimberlite melt itself was the metasomatizing agent.

Our research demonstrates that the modest isotopic variations reported in mantle peridotites may contain overlooked signals of subduction processes over geologic time. By pairing stable isotope data with major and trace element geochemical data, we have identified metasomatism by subduction-derived fluids within the subcontinental lithospheric mantle. These results underscore the necessity of considering the impact of subducted materials on the mantle's geochemical evolution, independent of specific geographic contexts. By focusing on the broader geochemical processes at play, this study contributes to the global understanding of mantle metasomatism and the geochemical evolution of the Earth's interior.

Data availability

Data are available through the Texas Data Repository at https://doi.org/10.18738/T8/5KITXN.

CRediT authorship contribution statement

S.E. Brooker: Writing – original draft, Visualization, Validation, Investigation. **J.D. Barnes:** Writing – review & editing, Visualization, Supervision, Resources, Project administration, Funding acquisition. **J. C. Lassiter:** Writing – review & editing, Visualization, Funding acquisition, Conceptualization. **A. Satkoski:** Writing – review & editing, Methodology, Formal analysis, Data curation. **D.G. Pearson:** Writing – review & editing, Visualization, Resources.

Declaration of competing interest

The authors declare that they have no known competing financial interests or personal relationships that could have appeared to influence the work reported in this paper.

Acknowledgments

This work constitutes part of the M.S. thesis of S. Brooker. Partial support and funding were provided by a GSA grant to S. Brooker, NSF grants EAR-1850749 and EAR-2234385 to J.D.B. and J.C.L., and funding from the Jackson School of Geosciences. The authors thank J. Cullen for help with oxygen and hydrogen isotope analyses. Constructive comments by Emily Chin and two anonymous reviewers improved this manuscript. We also thank Ralf Halama and Jeffrey Catalano for efficient editorial handling.

Appendix A. Supplementary material

Supplementary material to this article can be found online at https://doi.org/10.1016/j.gca.2024.09.036.

References

Alt, J.C., Muehlenbachs, K., Honnorez, J., 1986. An oxygen isotopic profile through the upper kilometer of the oceanic crust, DSDP Hole 504B. Earth Planet. Sci. Lett. 80, 217–229.
Amsellem, E., Moynier, F., Puchtel, I.S., 2019. Evolution of the Ca isotopic composition of the mantle. Geochim. Cosmochim. Acta 258, 195–206.
Amsellem, E., Moynier, F., Bouyon, A., Mata, J., Tappe, S., Day, J.D., 2020. Calcium isotopic evidence for the mantle sources of carbonatites. Sci. Adv. 6, 1–6.
Antonelli, M.A., Schiller, M., Schauble, E.A., Mittal, T., DePaolo, D.J., Chacko, T., Grew, E.S., Tripoli, B., 2019. Kinetic and equilibrium Ca isotope effects in high-T rocks and minerals. Earth Planet. Sci. Lett. 517, 71–82.
Antonelli, M.A., Giuliani, A., Wang, Z., Wang, M., Zhou, L., Feng, L., Li, M., Zhang, Z., Liu, F., Drysdale, R.N., 2023. Subducted carbonates not required: deep mantle melting explains stable Ca isotopes in kimberlite magmas. Geochim. Cosmochim. Acta 348, 410–427.
Araújo, D.P., Griffin, W.L., O'Reilly, S.Y., 2009. Mantle melts, metasomatism and diamond formation: insights from melt inclusions in xenoliths from Diavik. Slave Craton: Lithos 112, 675–682.
Aulbach, S., Creaser, R.A., Pearson, N.J., Simonetti, S.S., Heaman, L.M., Griffin, W.L., Stachel, T., 2009. Sulfide and whole rock Re–Os systematics of eclogite and pyroxenite xenoliths from the Slave Craton, Canada. Earth Planet. Sci. Lett. 283, 48–58.
Aulbach, S., Griffin, W.L., Pearson, N.J., O'Reilly, S.Y., Kivi, K., Doyle, B.J., 2004, Mantle formation and evolution, Slave Craton: constraints from HSE abundances and Re–Os isotope systematics of sulfide inclusions in mantle xenocrysts: Highly Siderophile Element Behavior in High Temperature Processes, 208, 61–88.
Aulbach, S., Pearson, N.J., O'Reilly, S.Y., Doyle, B.J., 2007. Origins of xenolithic eclogites and pyroxenites from the central slave Craton, Canada. J. Petrol. 48, 1843–1873.
Aulbach, S., Griffin, W.L., Pearson, N.J., O'Reilly, S.Y., 2013. Nature and timing of metasomatism in the stratified mantle lithosphere beneath the central Slave craton (Canada). Chem. Geol. 352, 153–169.
Bach, W., Alt, J.C., Niu, Y., Humphris, S.E., Erzinger, J., Dick, H.J.B., 2001. The geochemical consequences of late-stage low-grade alteration of lower ocean crust at the SW Indian Ridge: results from ODP Hole 735B (Leg 176). Geochim. Cosmochim. Acta v. 65, 3267–3287.
Banerjee, S., Kyser, T.K., Mitchell, R.H., 2018. Oxygen and hydrogen isotopic composition of phlogopites and amphiboles in diamond-bearing kimberlite hosted MARID xenoliths: constraints on fluid-rock interaction and recycled crustal material in the deep continental lithospheric mantle. Chem. Geol. 479, 272–285.
Bindeman, I.N., Ionov, D.A., Tollen, P.M.E., Golovin, A.V., 2022. Oxygen isotope ($\delta^{18}O$, $\Delta'^{17}O$) insights into continental mantle evolution since the Archean. Nat. Commun. 13, 1–10.
Blättler, C.L., Higgins, J.A., 2017. Testing Urey's carbonate–silicate cycle using the calcium isotopic composition of sedimentary carbonates. Earth Planet. Sci. Lett. 479, 241–251.
Boettcher, A.L., O'Neil, J.R., 1980. Stable isotope, chemical, and petrograohic studies of high-pressure amphiboles and micas: evidence for metasomatism in the mantle source regions of alkali basalts and kimberlites. Am. J. Sci. v. 280-A, 594–621.
Brey, G.P., Köhler, T., 1990. Geothermobarometry in Four-phase Lherzolites II. New thermobarometers, and practical assessment of existing thermobarometers. J. Petrol. 31, 1353–1378.
Carbno, G.B., Canil, D., 2002. Mantle structure beneath the SW Slave Craton, Canada: constraints from garnet geochemistry in the drybones bay kimberlite. J. Petrol. 43, 129–142.
Chazot, G., Lowry, D., Menzies, M., Mattey, D., 1997. Oxygen isotopic composition of hydrous and anhydrous mantle peridotites. Geochim. Cosmochim. Acta 61, 161–169.
Chen, C., Liu, Y., Feng, L., Foley, S.F., Zhou, L., Ducea, M.N., Hu, Z., 2018. Calcium isotope evidence for subduction-enriched lithospheric mantle under the northern North China Craton. Geochim. Cosmochim. Acta 238, 55–67.
Chen, C., Dai, W., Wang, Z., Liu, Y., Li, M., Becker, H., Foley, S.F., 2019. Calcium isotope fractionation during magmatic processes in the upper mantle. Geochim. Cosmochim. Acta 249, 121–137.
Chiba, H., Chacko, T., Clayton, R.N., Goldsmith, J.R., 1989. Oxygen isotope fractionations involving diopside, forsterite, magnetite, and calcite: application to geothermometry. Geochim. Cosmochim. Acta 53, 2985–2995.
Crank, J., 1979. The Mathematics of Diffusion. Clarendon Press, p. 428.
Creaser, R.A., Grütter, H., Carlson, J., Crawford, B., 2004. Macrocrystal phlogopite Rb–Sr dates for the Ekati property kimberlites, Slave Province, Canada: evidence for multiple intrusive episodes in the Paleocene and Eocene: Selected Papers from the Eighth International Kimberlite Conference. Volume 1. The C Roger Clement 76, 399–414.
Creighton, S., Stachel, T., Eichenberg, D., Luth, R., 2010. Oxidation state of the lithospheric mantle beneath Diavik diamond mine, central Slave craton, NWT, Canada | SpringerLink. Contrib. Miner. Petrol. 159, 645–657.
Crough, S.T., Morgan, W.J., Hargraves, R.B., 1980. Kimberlites: their relation to mantle hotspots. Earth Planet. Sci. Lett. 50, 260–274.

Currie, C.A., Beaumont, C., 2011. Are diamond-bearing Cretaceous kimberlites related to low-angle subduction beneath western North America? Earth Planet. Sci. Lett. 303, 59–70.
Dai, W., Wang, Z., Liu, Y., Chen, C., Zong, K., Zhou, L., Zhang, G., Li, M., Moynier, F., Hu, Z., 2020. Calcium isotope compositions of mantle pyroxenites. Geochim. Cosmochim. Acta 270, 144–159.
Dallai, L., Bianchini, G., Avanzinelli, R., Natali, C., Conticelli, S., 2019. Heavy oxygen recycled into the lithospheric mantle. Sci. Rep. 9, 1–7.
Dégi, J., Abart, R., Török, K., Bali, E., Wirth, R., Rhede, D., 2010. Symplectite formation during decompression induced garnet breakdown in lower crustal mafic granulite xenoliths: mechanisms and rates. Contrib. Miner. Petrol. 159, 293–314.
Deines, P., Haggerty, S.E., 2000. Small-scale oxygen isotope variations and petrochemistry of ultradeep (>300 km) and transition zone xenoliths. Geochim. Cosmochim. Acta 64, 117–131.
Dongre, A.N., Viljoen, K.S., Rao, N.V.C., Gucsik, A., 2016. Origin of Ti-rich garnets in the groundmass of Wajrakarur field kimberlites, southern India: insights from EPMA and Raman spectroscopy. Mineral. Petrol. 110, 295–307.
Eiler, J.M., 2001. Oxygen isotope variations of basaltic lavas and upper mantle rocks. Rev. Mineral. Geochem. 43, 319–364.
Eriksen, Z.T., Jacobsen, S.B., Day, J.M.D., White, W.M., 2024. Calcium isotope variability among ocean islands reveals the physical and lithological controls on mantle partial melting. Geochim. Cosmochim. Acta 373, 326–341.
Fantle, M.S., Tipper, E.T., 2014. Calcium isotopes in the global biogeochemical Ca cycle: implications for development of a Ca isotope proxy. Earth Sci. Rev. 129, 148–177.
Fedortchuk, Y., Canil, D., 2004. Intensive variables in kimberlite magmas, Lac de Gras, Canada and implications for diamond survival. J. Petrol. 45, 1725–1745.
Fitzpayne, A., Giuliani, A., Harris, C., Thomassot, E., Cheng, C., Hergt, J., 2019. Evidence for subduction-related signatures in the southern African lithosphere from the N-O isotopic composition of metasomatic mantle minerals. Geochim. Cosmochim. Acta 266, 237–257.
Godard, G., Martin, S., 2000. Petrogenesis of kelyphites in garnet peridotites: a case study from the Ulten zone, Italian Alps. J. Geodynam. 30, 117–145.
Graham, I., Burgess, J., Bryan, D., Ravenscroft, P., Thomas, E., Doyle, B., Hopkins, R., Armstrong, K., 1999. Exploration history and geology of the Diavik kimberlites, Lac de Gras, Northwest Territories, Canada, *in* v. 1, p. 262–279.
Gregory, R.T., Taylor, H.P., 1981. An oxygen isotope profile in a section of Cretaceous oceanic crust, Samail Ophiolite, Oman: evidence for δ18O buffering of the oceans by deep (>5 km) seawater-hydrothermal circulation at mid-ocean ridges. J. Geophys. Res. Solid Earth 86, 2737–2755.
Gregory, R.T., Taylor, H.P., 1986. Possible non-equilibrium oxygen isotope effects in mantle nodules, an alternative to the Kyser-O'Neil-Carmichael18O/16O geothermometer. Contrib. Miner. Petrol. 93, 114–119.
Griffin, W.L., Doyle, B.J., Ryan, C.G., Pearson, N.J., Suzanne, Y.O., Davies, R., Kivi, K., Van Achterbergh, E., Natapov, L.M., 1999a. Layered mantle lithosphere in the Lac de Gras Area, Slave Craton: composition, structure and origin. J. Petrol. 40, 705–727.
Griffin, W.L., O'Reilly, S.Y., Ryan, C.G., 1999b. The composition and origin of subcontinental lithospheric mantle. In: Mantle Petrology: Field Observations and High Pressure Experimentation: A Tribute to Francis R. (Joe) Boyd. Geochemical Society, Houston, Geochem. Soc. Spec. Publ., pp. 13–45
Grütter, H., Apter, D.B., Kong, J., 1999, Crust-mantle coupling: evidence from mantle-derived xenocrystic garnets: In Proceedings of the VIIth International Kimberlite Conference. Cape Town, pp. 307–313.
Guiliani, A., Martin, L.A.J., Soltys, A., Griffin, W.L., 2019. Mantle-like oxygen isotopes in kimberlites determined by in situ SIMS analyses of zoned olivine. Geochim. Cosmochim. Acta 266, 274–291.
Hao, Y., Xia, Q., Dallai, L., Coltorti, M., 2015. Recycled oceanic crust-derived fluids in the lithospheric mantle of eastern China: constraints from oxygen isotope compositions of peridotite xenoliths. Lithos 228–229, 55–61.
Hauri, E., 2002. SIMS analysis of volatiles in silicate glasses, 2: isotopes and abundances in Hawaiian melt inclusions. Chem. Geol. 183, 115–141.
He, Y., Wang, Y., Zhu, C., Huang, S., Li, S., 2017. Mass-independent and mass-dependent Ca isotopic compositions of thirteen geological reference materials measured by thermal ionisation mass spectrometry. Geostand. Geoanal. Res. 41, 283–302.
Heaman, L.M., Kjarsgaard, B.A., and Creaser, R.A., 2003. The timing of kimberlite magmatism in North America: implications for global kimberlite genesis and diamond exploration: a tale of two cratons. In: The Slave-Kaapvaal Workshop, vol. 71, p. 153–184.
Heaman, L.M., Pearson, D.G., 2010. Nature and evolution of the Slave Province subcontinental lithospheric mantle. This article is one of a series of papers published in this Special Issue on the theme Lithoprobe — parameters, processes, and the evolution of a continent (R. Clowes, Ed.). Can. J. Earth Sci. 47, 369–388.
Helmstaedt, H., 2009. Crust–mantle coupling revisited: The Archean Slave craton, NWT, Canada. In: Proceedings of the 9th International Kimberlite Conference, vol. 112, p. 1055–1068.
Horstmann, U.E., Verwoerd, W.J., 1997. Carbon and oxygen isotope variations in southern African carbonatites. J. Afr. Earth Sc. 25, 115–136.
Huang, S., Farkas, J., Jacobsen, S.B., 2010. Calcium isotopic fractionation between clinopyroxene and orthopyroxene from mantle peridotites. Earth Planet. Sci. Lett. 292, 337–344.
Huang, F., Zhou, C., Wang, W., Kang, J., Wu, Z., 2019. First-principles calculations of equilibrium Ca isotope fractionation: implications for oldhamite formation and evolution of lunar magma ocean. Earth Planet. Sci. Lett. 510, 153–160.
Humphreys, E., Hessler, E., Dueker, K., Farmer, G.L., Erslev, E., Atwater, T., 2003. How laramide-age hydration of North American lithosphere by the farallon slab controlled subsequent activity in the western United States. Int. Geol. Rev. 45, 575–595.
Ingrin, J., Pacaud, L., Jaoul, O., 2001. Anisotropy of oxygen diffusion in diopside. Earth Planet. Sci. Lett. 192, 347–361.
Ionov, D.A., Harmon, R.S., France-Lanord, C., Greenwood, P.B., Ashchepkov, I.V., 1994. Oxygen isotope composition of garnet and spinel peridotites in the continental mantle: evidence from the Vitim xenolith suite, southern Siberia. Geochim. Cosmochim. Acta 58, 1463–1470.
Ionov, D.A., Qi, Y.-H., Kang, J.-T., Golovin, A.V., Oleinikov, O.B., Zheng, W., Anbar, A.D., Zhang, Z.-F., Huang, F., 2019. Calcium isotopic signatures of carbonatite and silicate metasomatism, melt percolation and crustal recycling in the lithospheric mantle. Geochim. Cosmochim. Acta 248, 1–13.
Irvine, G.J., 2002. Time Constraints on the Formation of Lithospheric Mantle beneath Cratons: A Re–Os Isotope and Platinum Group Element Study of Peridotite Xenoliths from Northern Canada and Lesotho. University of Durham, Durham, p. 384 pp.. PhD Thesis.
Isachsen, C.E., Bowring, S.A., 1994. Evolution of the Slave craton. Geology 22, 917.
John, T., Gussone, N., Podladchikov, Y.Y., Bebout, G.E., Dohmen, R., Halama, R., Klemd, R., Magna, T., Seitz, H.-M., 2012. Volcanic arcs fed by rapid pulsed fluid flow through subducting slabs. Nat. Geosci. 5, 489–492.
Kamenetsky, V.S., Grütter, H., Kamenetsky, M.B., Gömann, K., 2013. Parental carbonatitic melt of the Koala kimberlite (Canada): constraints from melt inclusions in olivine and Cr-spinel, and groundmass carbonate. Chem. Geol. 353, 96–111.
Kang, J.-T., Zhu, H.-L., Liu, Y.-F., Liu, F., Wu, F., Hao, Y.-T., Zhi, X.-C., Zhang, Z.-F., Huang, F., 2016. Calcium isotopic composition of mantle xenoliths and minerals from Eastern China. Geochim. Cosmochim. Acta 174, 335–344.
Kang, J.-T., Ionov, D.A., Liu, F., Zhang, C.-L., Golovin, A.V., Qin, L.-P., Zhang, Z.-F., Huang, F., 2017. Calcium isotopic fractionation in mantle peridotites by melting and metasomatism and Ca isotope composition of the Bulk Silicate Earth. Earth Planet. Sci. Lett. v. 474, 128–137.
Kang, J.-T., Ionov, D.A., Zhu, H.-L., Liu, F., Zhang, Z.-F., Liu, Z., Huang, F., 2019. Calcium isotope sources and fractionation during melt-rock interaction in the lithospheric mantle: EVIDENCE from pyroxenites, wehrlites, and eclogites. Chem. Geol. 524, 272–282.
Kang, J.-T., Zhou, C., Huang, J.-Y., Hao, Y.-T., Liu, F., Zhu, H.-L., Zhang, Z.-F., Huang, F., 2020. Diffusion-driven Ca-Fe isotope fractionations in the upper mantle: implications for mantle cooling and melt infiltration. Geochim. Cosmochim. Acta 290, 41–58.
Kelley, K.A., Plank, T., Ludden, J., Staudigel, H., 2003. Composition of altered oceanic crust at ODP sites 801 and 1149. Geochem., Geophys., Geosyst. 4.
Kilgore, M.L., et al., 2020. Metasomatic control of hydrogen contents in the layered cratonic mantle lithosphere sampled by Lac de Gras xenoliths in the central Slave craton, Canada. Geochim. Cosmochim. Acta 286, 29–53.
Kjarsgaard, B., 2007. Kimberlite pipe models: significance for exploration. In: Proceedings of Exploration 07: Fifth Decennial International Conference on Mineral Exploration.
Klein-BenDavid, O., Logvinova, A.M., Schrauder, M., Spetius, Z.V., Weiss, Y., Hauri, E.H., Kaminsky, F.V., Sobolev, N.V., Navon, O., 2009. High-Mg carbonatitic microinclusions in some Yakutian diamonds—a new type of diamond-forming fluid. Lithos 112, 648–659.
Kopylova, M.G., McCammon, C., 2003, Composition and the redox state of the Slave peridotitic mantle. In: 8th International Kimberlite Conference Long Abstracts, pp. 1–5.
Kopylova, M.G., Russell, J.K., 2000. Chemical stratification of cratonic lithosphere: constraints from the Northern Slave craton, Canada. Earth Planet. Sci. Lett. 181, 71–87.
Kuroda, Y., Suzuoki, T., Matsuo, S., Aoki, K., 1975. ichiro, D/H ratios of the coexisting phlogopite and richterite from mica nodules and a peridotite in South African kimberlites. Contrib. Miner. Petrol. 52, 315–318.
Kuroda, Y., Suzuoki, T., Matsuo, S., 1977. Hydrogen isotope composition of deep-seated water. Contrib. Miner. Petrol. 60, 311–315.
Kyser, T.K., O'Neil, J.R., 1984. Hydrogen isotope systematics of submarine basalts. Geochim. Cosmochim. Acta 48, 2123–2133.
Lebedeva, N.M., Nosova, A.A., Kargin, A.V., Larionova, Y.O., Sazonova, L.V., Tikhomirova, Y.S., 2020. Sr–Nd–O isotopic evidence of variable sources of mantle metasomatism in the subcratonic lithospheric mantle beneath the Grib kimberlite, northwestern Russia. Lithos 376–377, 105779.
Lecuyer, C., Reynard, B., 1996. High-temperature alteration of oceanic gabbros by seawater (Hess Deep, Ocean Drilling Program Leg 147): evidence from oxygen isotopes and elemental fluxes. J. Geophys. Res. 101, 15883–15897.
Lee, C.A., 2005. Trace element evidence for hydrous metasomatism at the base of the North American lithosphere and possible association with laramide low-angle subduction. J. Geol. 113, 673–685.
Liu, L., Gurnis, M., Seton, M., Saleeby, J., Müller, R.D., Jackson, J.M., 2010. The role of oceanic plateau subduction in the Laramide orogeny. Nat. Geosci. 3, 353–357.
Liu, F., Li, X., Wang, G., Liu, Y., Zhu, H., Kang, J., Huang, F., Sun, W., Xia, X., Zhang, Z., 2017. Marine carbonate component in the mantle beneath the southeastern Tibetan plateau: evidence from magnesium and calcium isotopes. J. Geophys. Res. Solid Earth 122, 9729–9744.
Liu, J., Pearson, D.G., Wang, L.H., Mather, K.A., Kjarsgaard, B.A., Schaeffer, A.J., Irvine, G.J., Kopylova, M.G., Armstrong, J.P., 2021. Plume-driven recratonization of deep continental lithospheric mantle. Nature 592, 732–736.
Liu, C.-Z., Wu, F.-Y., Chung, S.-L., Li, Q.-L., Sun, W.-D., Ji, W.-Q., 2014. A 'hidden' 18O-enriched reservoir in the sub-arc mantle. Sci. Rep. 4, 1–6.
Lowry, D., Mattey, D.P., Harris, J.W., 1999. Oxygen isotope composition of syngenetic inclusions in diamond from the Finsch Mine, RSA. Geochim. Cosmochim. Acta 63, 1825–1836.

Magna, T., Gussone, N., Mezger, K., 2015. The calcium isotope systematics of Mars. Earth Planet. Sci. Lett. v. 430, 86–94.
Marshall, E.W., Barnes, J.D., Lassiter, J.C., 2017. The role of serpentinite-derived fluids in metasomatism of the Colorado Plateau (USA) lithospheric mantle. Geology 45, 1103–1106.
Mattey, D., Lowry, D., Macpherson, C., 1994. Oxygen isotope composition of mantle peridotite. Earth Planet. Sci. Lett. 128, 231–241.
McDonough, W.F., Sun, S.-S., 1995. The composition of the Earth. Chem. Geol. 120, 223–253.
Mitchell, R.H., 2013. Kimberlites: Mineralogy, Geochemistry, and Petrology. Springer Science & Business Media, p. 453.
Mozley, P.S., Burns, S.J., 1993. Oxygen and carbon isotopic composition of marine carbonate concretions; an overview. J. Sediment. Res. 63, 73–83.
Navon, O., Klein-BenDavid, O., Weiss, Y., 2008, Diamond-forming fluids: their origin and evolution, *in* v. 9.
Obata, M., 1994. Material transfer and local equilibria in a zoned kelyphite from a garnet pyroxenite, Ronda, Spain. J. Petrol. 35, 271–287.
Orr, P., Luth, R.W., 2000. Petrology and oxygen-isotope geochemistry of the Yamba Lake kimberlite rocks, N.W.T. Can. J. Earth Sci. 37, 1053–1071.
Pearson, D.G., 1999. The age of continental roots. Lithos 48, 171–194.
Pearson, N.J., Griffin, W.L., Doyle, B.J., O'Reilly, S.Y., Van Achterbergh, Kivi, K., 1999. k: Proceedings of the VIIth International Kimberlite Conference, Cape Town, pp. 670–672.
Perkins, G.B., Sharp, Z.D., Selverstone, J., 2006. Oxygen isotope evidence for subduction and rift-related mantle metasomatism beneath the Colorado Plateau-Rio Grande rift transition. Contrib. Miner. Petrol. 151, 633.
Phipps, S.P., 1988. Deep rifts as sources for alkaline intraplate magmatism in eastern North America. Nature 334, 27–31.
Pokhilenko, L., 2021. Kelyphite rims on garnets of contrast parageneses in mantle xenoliths from the Udachnaya-East kimberlite pipe (Yakutia). Minerals 11, 615.
Polat, A., Frei, R., Longstaffe, F.J., Thorkelson, D.J., Freidman, E., 2018. Petrology and geochemistry of the Tasse mantle xenoliths of the Canadian Cordillera: a record of Archean to Quaternary mantle growth, metasomatism, removal, and melting. Tectonophysics 737, 1–26.
Price, S.E., Russell, J.K., Kopylova, M.G., 2000. Primitive magma from the Jericho Pipe, N.W.T., Canada: constraints on primary kimberlite melt chemistry. J. Petrol. 41, 789–808.
Regier, M.E., Mišković, A., Ickert, R.B., Pearson, D.G., Stachel, T., Stern, R.A., Kopylova, M., 2018. An oxygen isotope test for the origin of Archean mantle roots. Geochem. Perspect. Lett. 45, 6–10.
Rehfeldt, T., Foley, S.F., Jacob, D.E., Carlson, R.W., Lowry, D., 2008. Contrasting types of metasomatism in dunite, wehrlite and websterite xenoliths from Kimberley, South Africa. Geochim. Cosmochim. Acta 72, 5722–5756.
Ringwood, A., Kesson, S., Hibberson, W., Ware, N., 1992. Origin of kimberlites and related magmas. Earth Planet. Sci. Lett. 113, 521–538.
Rosenbaum, J.M., Walker, D., Kyser, T.K., 1994. Oxygen isotope fractionation in the mantle. Geochim. Cosmochim. Acta 58, 4767–4777.
Rudge, J.F., Reynolds, B.C., Bourdon, B., 2009. The double spike toolbox. Chem. Geol. 265, 420–431.
Russell, J.K., Porritt, L.A., Lavallée, Y., Dingwell, D.B., 2012. Kimberlite ascent by assimilation-fuelled buoyancy. Nature 481, 352–356.
Safonov, O., Chertkova, N., Perchuk, L., Litvin, Y.A., 2009. Experimental model for alkalic chloride-rich liquids in the upper mantle. Lithos 112, 260–273.
Sarkar, C., Heaman, L.M., Pearson, D.G., 2015. Duration and periodicity of kimberlite volcanic activity in the Lac de Gras kimberlite field, Canada and some recommendations for kimberlite geochronology. Lithos 218–219, 155–166.
Schmidberger, S.S., Heaman, L.H., Simonetti, A., Creaser, R.A., Cookenboo, H., 2005. Formation of Paleoproterozoic eclogitic mantle, Slave Province (Canada): insights from in-situ Hf and U-Pb isotopic analyses of mantle zircons. Earth Planet. Sci. Lett. 240, 621–633.
Schmidberger, S.S., Simonetti, A., Heaman, L.H., Creaser, R.A., Whiteford, S., 2007. Lu–hf, in-situ Sr and Pb Isotope and trace element systematics for mantle eclogites from the diavik diamond mine: evidence for paleoproterozoic subduction beneath the slave craton, Canada. Earth Planet. Sci. Lett. 254, 55–68.
Sharp, Z.D., 1990. A laser-based microanalytical method for the in situ determination of oxygen isotope ratios of silicates and oxides. Geochim. Cosmochim. Acta 54, 1353–1357.
Sharp, Z., 2017. Principles of Stable Isotope Geochemistry, second ed. Open Textbooks.
Sharp, Z.D., Atudorei, V., Durakiewicz, T., 2001. A rapid method for determination of hydrogen and oxygen isotope ratios from water and hydrous minerals. Chem. Geol. 178, 197–210.
Sharygin, I.S., Litasov, K.D., Shatskiy, A., Safonov, O.G., Golovin, A.V., Ohtani, E., Pokhilenko, N.P., 2017, Experimental constraints on orthopyroxene dissolution in alkali-carbonate melts in the lithospheric mantle: Implications for kimberlite melt composition and magma ascent: the role of intraplate magmas and their inclusions in Earth's mantle evolution, 455, 44–56.
Shaw, A.M., Hauri, E.H., Fischer, T.P., Hilton, D.R., Kelley, K.A., 2008. Hydrogen isotopes in Mariana arc melt inclusions: Implications for subduction dehydration and the deep-Earth water cycle. Earth Planet. Sci. Lett. 275, 138–145.
Shephard, G.E., Flament, N., Williams, S., Seton, M., Gurnis, M., Müller, R.D., 2014. Circum-Arctic mantle structure and long-wavelength topography since the Jurassic. J. Geophys. Res.: Solid Earth 119, 7889–7908.
Sheppard, S.M.F., Dawson, J.B., 1975. Hydrogen, carbon, and oxygen istope studies of megacryst and matrix minerals from Lesothan and South African kimberlites. In: Ahrens, L.H., Dawson, J.B., Duncan, A.R., Erlank, A.J. (Eds.), Physics and Chemistry of the Earth. Pergamon, pp. 747–763.
Sheppard, S.M.F., Epstein, S., 1970. D/H and18O/16O ratios of minerals of possible mantle or lower crustal origin. Earth Planet. Sci. Lett. 9, 232–239.
Shilobreeva, S., Martinez, I., Busigny, V., Agrinier, P., Laverne, C., 2011. Insights into C and H storage in the altered oceanic crust: results from ODP/IODP Hole 1256D. Geochim. Cosmochim. Acta 75, 2237–2255.
Shu, Q., Brey, G.P., 2015. Ancient mantle metasomatism recorded in subcalcic garnet xenocrysts: temporal links between mantle metasomatism, diamond growth and crustal tectonomagmatism. Earth Planet. Sci. Lett. 418, 27–39.
Smart, K.A., Chacko, T., Simonetti, A., Sharp, Z.D., Heaman, L.H., 2014. A record of paleoproterozoic subduction preserved in the northern slave cratonic mantle: Sr–Pb–O isotope and trace-element investigations of eclogite xenoliths from the Jericho and Muskox kimberlites. J. Petrol. 55, 549–583.
Smart, K.A., Tappe, S., Simonetti, A., Simonetti, S.S., Woodland, A.B., Harris, C., 2017. Tectonic significance and redox state of Paleoproterozoic eclogite and pyroxenite components in the Slave cratonic mantle lithosphere, Voyageur Kimberlite, Arctic Canada. Chem. Geol. 455, 98–119.
Smart, K.A., Tappe, S., Woodland, A.B., Greyling, D.R., Harris, C., Gussone, N., 2021. Constraints on Archean crust recycling and the origin of mantle redox variability from the δ44/40Ca – δ18O – fO2 signatures of cratonic eclogites. Earth Planet. Sci. Lett. 556, 116720.
Smith, D., 2010. Antigorite peridotite, metaserpentinite, and other inclusions within diatremes on the Colorado Plateau, SW USA: implications for the mantle wedge during low-angle subduction. J. Petrol. 51, 1355–1379.
Sobolev, N.V., Lavrent'ev, Ju.G., 1971. Isomorphic sodium admixture in garnets formed at high pressures. Contrib. Miner. Petrol. 31, 1–12.
Soderman, C.R., Matthews, S., Shorttle, O., Jackson, M.G., Ruttor, S., Nebel, O., Turner, S., Beier, C., Millet, M.-A., Widom, E., Humayun, M., Williams, H.M., 2021. Heavy δ^{57}Fe in ocean island basalts: a non-unique signature of processes and source lithologies in the mantle. Geochim. Cosmochim. Acta 292, 309–332.
Soltys, A., Giuliani, A., Phillips, D., Kamenetsky, V.S., Maas, R., Woodhead, J., Rodemann, T., 2016. In-situ assimilation of mantle minerals by kimberlitic magmas – direct evidence from a garnet wehrlite xenolith entrained in the Bultfontein kimberlite (Kimberley, South Africa). Lithos 256–257, 182–196.
Staudigel, H., Davies, G.R., Hart, S.R., Marchant, K.M., Smith, Brian M., 1995. Large scale isotopic Sr, Nd and O isotopic anatomy of altered oceanic crust: DSDP/ODP sites417/418. Earth Planet. Sci. Lett. 130, 169–185.
Tappe, S., Graham Pearson, D., Kjarsgaard, B.A., Nowell, G., Dowall, D., 2013. Mantle transition zone input to kimberlite magmatism near a subduction zone: origin of anomalous Nd–hf isotope systematics at Lac De Gras, Canada. Earth Planet. Sci. Lett. 371–372, 235–251.
Tappe, S., Massuyeau, M., Smart, K.A., Woodland, A.B., Gussone, N., Milne, S., Stracke, A., 2021. Sheared peridotite and megacryst formation beneath the kaapvaal craton: a snapshot of tectonomagmatic processes across the lithosphere-asthenosphere transition. J. Petrol. 62, 1–39.
Torsvik, T.H., Burke, K., Steinberger, B., Webb, S.J., Ashwal, L.D., 2010. Diamonds sampled by plumes from the core–mantle boundary. Nature 466, 352–355.
Valley, J.W., 2003. Oxygen isotopes in zircon. Rev. Mineral. Geochem. 53, 343–385.
Valley, J.W., Kitchen, N., Kohn, M.J., Niendorf, C.R., Spicuzza, M.J., 1995. UWG-2, a garnet standard for oxygen isotope ratios: strategies for high precision and accuracy with laser heating. Geochim. Cosmochim. Acta 59, 5223–5231.
Walowski, K.J., Wallace, P.J., Hauri, E.H., Wada, I., Clynne, M.A., 2015. Slab melting beneath the Cascade Arc driven by dehydration of altered oceanic peridotite. Nat. Geosci. 8, 404–408.
Wang, Z., Bucholz, C., Skinner, B., Shimizu, N., Eiler, J., 2011. Oxygen isotope constraints on the origin of high-Cr garnets from kimberlites. Earth Planet. Sci. Lett. 312, 337–347.
Wang, Y., He, Y., Wu, H., Zhu, C., Huang, S., Huang, J., 2019. Calcium isotope fractionation during crustal melting and magma differentiation: granitoid and mineral-pair perspectives. Geochim. Cosmochim. Acta 259, 37–52.
Wang, S.-J., Teng, F.-Z., Scott, J.M., 2016. Tracing the origin of continental HIMU-like intraplate volcanism using magnesium isotope systematics. Geochim. Cosmochim. Acta 185, 78–87.
Wang, C.-G., Xu, W.-L., Yang, D.-B., Liu, Y.-S., Pei, F.-P., Li, Q.-L., Zhou, Q.-J., 2018. Olivine oxygen isotope evidence for intracontinental recycling of delaminated continental crust. Geochem., Geophys., Geosyst. 19, 1913–1924.
Weiss, Y., Kessel, R., Griffin, W., Kiflawi, I., Klein-BenDavid, O., Bell, D., Harris, J., Navon, O., 2009. A new model for the evolution of diamond-forming fluids: evidence from microinclusion-bearing diamonds from Kankan, Guinea. Lithos 112, 660–674.
Weiss, Y., McNeill, J., Pearson, D.G., Nowell, G.M., Ottley, C.J., 2015. Highly saline fluids from a subducting slab as the source for fluid-rich diamonds. Nature 524, 339–342.
Wenner, D.B., Taylor, H.P., 1974. D/H and O18/O16 studies of serpentinization of ultramaflc rocks. Geochim. Cosmochim. Acta 38, 1255–1286.
Westerlund, K.J., Shirey, S.B., Richardson, S.H., Carlson, R.W., Gurney, J.J., Harris, J.W., 2006. A subduction wedge origin for Paleoarchean peridotitic diamonds and harzburgites from the Panda kimberlite, Slave craton: evidence from Re–Os isotope systematics. Contrib. Miner. Petrol. v. 152, 275–294.
Wilson, M.R., Kjarsgaard, B.A., Taylor, B., 2007. Stable isotope composition of magmatic and deuteric carbonate phases in hypabyssal kimberlite Lac De Gras Field, Northwest Territories, Canada. Chem. Geol. 242, 435–454.
Workman, R.K., Hart, S.R., 2005. Major and trace element composition of the depleted MORB mantle (DMM). Earth Planet. Sci. Lett. 231, 53–72.
Xu, J.Y., Guiliani, A., Li, Q.L., Lu, K., Melgarejo, J.C., Griffin, W.L., 2021. Light oxygen isotopes in mantle-derived magmas reflect assimilation of sub-continental lithospheric mantle material. Nat. Commun. 12, 1–13.

Zhang, H.-F., Mattey, D.P., Grassineau, N., Lowry, D., Brownless, M., Gurney, J.J., Menzies, M.A., 2000. Recent fluid processes in the Kaapvaal Craton, South Africa: coupled oxygen isotope and trace element disequilibrium in polymict peridotites. Earth Planet. Sci. Lett. 176, 57–72.
Zhao, X., Zhang, Z., Huang, S., Liu, Y., Li, X., Zhang, H., 2017. Coupled extremely light Ca and Fe isotopes in peridotites. Geochim. Cosmochim. Acta 208, 368–380.
Zheng, 1993. Calculation of oxygen isotope fractionation in anhydrous silicate minerals. Geochim. Cosmochim. Acta 57, 1079–1091.
Zhu, H., Liu, F., Li, X., Wang, G., Zhang, Z., Sun, W., 2018. Calcium isotopic compositions of normal mid-ocean ridge basalts from the southern Juan de Fuca Ridge. J. Geophys. Res. 123, 1303–1313.
Zou, Z., Wang, Z., Wang, X.-J., Xu, Y.-G., Chen, L.-H., Wang, M., Feng, L., Li, M., Liu, Y., 2024. Calcium isotopic compositions of eclogite melts and negligible modification during reaction with lithospheric mantle. Geochim. Cosmochim. Acta 367, 58–71.